CHAPTER 7: SEMICONDUCTOR PHOTOCATHODES FOR UNPOLARIZED ELECTRON BEAMS

IVAN BAZAROV

Physics Department
373 Wilson Laboratory
Cornell University
Ithaca, NY 14853

LUCA CULTRERA

Cornell Laboratory of Accelerator-based Sciences and Education
Cornell University
Ithaca, NY 14853

TRIVENI RAO

Brookhaven National Laboratory
Upton, NY 11973

Keywords

Photocathode, Semiconductor, Antimonide, Telluride, Multi-alkali, Cesium, GaAs, GaN, Quantum Efficiency, Life-Time, Intrinsic Emittance, Thermal Emittance, Response Time, Electron Affinity, Negative Electron Affinity, Cathode Fabrication, Cs_2Te Cathode, K_2CsSb Cathode, Cs_3Sb Cathode, Response Time, Activation, Surface Roughness, High-Current

Abstract

Semiconductor photocathodes offer great advantage for generating high average currents by the virtue of their high quantum efficiency in the UV or VIS spectral ranges. This chapter reviews basic properties of these photoemissive materials. Standard growth and preparation procedures for antimony and tellurium based alkali photocathodes as well as for III-V semiconductors activated to negative electron affinity are presented. Various technical requirements and instrumentation needed either for the synthesis or the activation of these materials are outlined.

7.1 PHOTOCATHODE TYPES

High quantum efficiency photocathodes are desirable for generating high average (greater than milliamperes) beam current. Essentially, all such photocathodes are semiconductors. Two general types of semiconductor photocathodes used in photoinjectors producing unpolarized electron beams are alkali-based ones (antimonides and tellurides), and bulk- or layered-III-V crystals (*e.g.*, GaAs or GaN) activated to the condition of negative electron affinity *via* the deposition of roughly a monolayer of cesium on the surface. In this chapter, we detail the important characteristics of these photocathodes, their growth procedures, and their performance in the accelerator environment.

7.2 DEFINITIONS AND PHOTOCATHODES' FIGURES OF MERIT

The intrinsic properties of the photocathode play a key role in establishing the quality of the electron beam (its emittance and time structure), the reliability of its operation, and the ease of maintenance.

The most relevant properties for a photocathode inside a photoinjector are its quantum efficiency and its spectral response, the photoemission response time, the thermal emittance (or intrinsic emittance), mean transverse energy, and the lifetime of the photocathode. Also of importance is its ability to withstand an adverse environment inside the photoemission gun, such as the back-streaming of ions, created *via* ionizing residual gas by the primary electron beam, towards the cathode. Its lifetime can also be negatively affected by residual gas inside the gun chamber. These effects determine the vacuum requirements for the photocathode (sensitivity to the partial pressure of various gasses encountered in ultra-high vacuum (UHV) systems) to maintain a high QE. Here, we summarize the main definitions used in this chapter.

Quantum efficiency (QE) is defined as the number of electrons per incident photon, given by the formula

$$\mathrm{QE} = \frac{I/e}{P/h\nu} \tag{7.1}$$

or, in practical units

$$\mathrm{QE}\ [\%] = 124\,\frac{I\ [\mathrm{A}]}{P\ [\mathrm{W}]\ \lambda\ [\mu\mathrm{m}]} \tag{7.2}$$

where I is the current emitted by the cathode, P is the laser power incident on the cathode, the electron charge e = 1.602×10^{-19} C, the Planck constant h = 6.626×10^{-34} Js, and, ν and λ are the frequency and wavelength of light, respectively. Other related definitions commonly used are spectral responsivity R (measured in units of ampere per Watt) and quantum yield (QY), defined as the number of electrons emitted per absorbed photon. For an optically opaque cathode, to convert QE to QY or to R, we use the following expressions

$$\mathrm{QY} = \mathrm{QE}\,\frac{1}{1-\varrho} \tag{7.3}$$

$$R\left[\frac{\mathrm{A}}{\mathrm{W}}\right] = \frac{\mathrm{QE}\ [\%]\ \lambda\ [\mu\mathrm{m}]}{124} \tag{7.4}$$

where ϱ is the reflectivity of the photocathode (on the scale of 0 to 1).

Spectral response, not to be confused with spectral responsivity, is a measure of QE as a function of the incident photon's wavelength. From the point of laser system and light-transport design, the preferred photocathodes have a good spectral response in the visible range.

Response time is defined as the time it takes for electrons excited by the incoming photons to escape from the cathode's surface. (Techniques for measuring the electron bunch length are detailed in Chapter 11.) The photocathode's response time is a critical parameter in producing very short electron pulses and for the temporal shaping of laser pulses required for a high brightness, low emittance beam.

7.2.1 Basic Band Gap Structure of Semiconductors

Semiconductors are characterized by having an energy structure wherein an energy gap separates the valence band (the highest occupied band) from the conduction band (the lowest empty band). Electrons are promoted from the valence to the conduction band by absorbing a photon of energy if $E_{ph} > E_{gap}$, where E_{ph} is the photon energy and E_{gap} is the gap energy. Electron affinity is defined as the difference between the vacuum energy level and the minimum of the conduction band. As depicted in Figure **7.1**, vacuum energy can lie either above the conduction band minimum (positive electron affinity), or below it (negative electron affinity). The three-step photoemission model, detailed in Chapter 5, [7.1] is also illustrated in the figure: 1) Photon absorption by an electron with its subsequent promotion from the valence band to the conduction band; 2) electron diffusion inside the crystal; and, 3) the electron's escape into the vacuum.

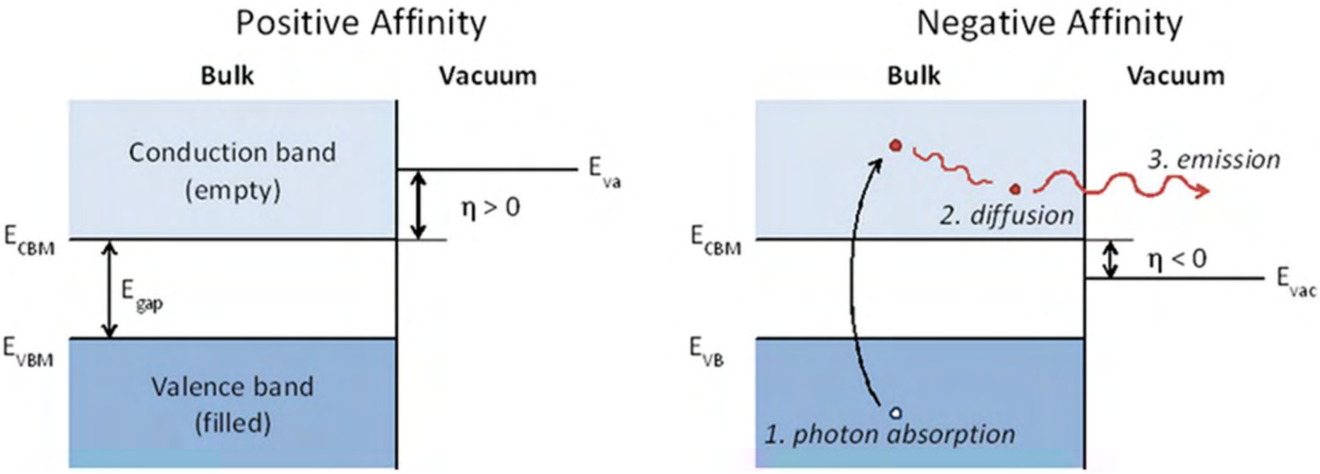

Figure 7.1. Basic semiconductor's energy structure of positive electron affinity (left) photocathode, and negative affinity (right) photocathode. Energy gap is defined as the difference between the conduction band minimum energy and the valence band maximum, $E_{gap} = E_{CBM} - E_{VBM}$. Electron affinity is defined as the difference between vacuum level energy and conduction band minimum, $\eta = E_{vac} - E_{CBM}$. The three-step Spicer photoemission model is also shown (right).

7.2.2 Transmission- and Reflection-Mode Photocathodes

Semiconductor photocathodes are realized in two basic configurations: Transmission- and reflection-mode. For the former, the laser light is coupled from the backplane of a thin film of photoemissive material deposited on a transparent substrate (typically glass, quartz, or sapphire). The film's thickness must be optimized to match the light's absorption length and the electrons' escape depth. The latter configuration can employ either a bulk crystal or a grown film. Most photoemission guns using high QE photocathodes have a translation mechanism that loads the photocathode from the back of the gun, and therefore, adopt the reflection-mode geometry of the photocathode.

Thermal emittance is defined as the photocathode's intrinsic emittance, *i.e.*, the emittance of the beam measured directly at the cathode in absence of any other degrading effects, such as aberrations from the electromagnetic fields of beam elements, or the space charge. The normalized root mean square (rms) thermal emittance of an electron beam in a direction transverse to the direction of propagation is defined as

$$\epsilon_{nx,th} = \sigma_x \sqrt{\frac{\mathrm{MTE}}{3m_0c^2}} \tag{7.5}$$

or, in practical units

$$\epsilon_{nx,th}\ [\mathrm{mm\ mrad}] = 1.40\sigma_x\ [\mathrm{mm}]\ \sqrt{\mathrm{MTE}\ [\mathrm{eV}]} \tag{7.6}$$

Here σ_x is the transverse rms spot size of the electron beam (same as the laser spot with a uniform QE distribution), MTE is the mean transverse energy, defined as MTE = $\langle ½m_0v_x^2\rangle + \langle ½m_0v_y^2\rangle$, with x and y denoting the directions perpendicular to the cathode's emission normal, and, m_0c^2 = 0.511 MeV is the electron's rest energy. The mean transverse energy, the average energy of the electrons in the transverse directions, is related to the mean transverse velocity spread of the beam. Unlike thermal emittance, which depends on the size of the laser spot, MTE is an intrinsic property of the photocathode and its condition at the surface. The significance of thermal emittance and the MTE is that they set an upper bound on the beam's brightness for photoinjectors delivering short bunches, that is, pancake-shaped ones near the photocathode with a diameter much larger than the longitudinal extent of the bunch after the illumination by an individual laser pulse is over [7.2].

7.2.3 Lifetime and Vacuum Requirements

The lifetime and vacuum requirements typically are defined by the time it takes for the QE of the cathode to drop to 1/*e* times its initial value. Additionally, one differentiates between the dark lifetime for the cathode storage, and the operational lifetime during the beam delivery. The cathode material and the conditions of the vacuum chamber housing the photocathode influence the dark lifetime. The photocathodes also are preferentially sensitive to certain residual gasses and their lifetime can be reduced greatly *via* chemical poisoning. Here, the most problematic species are H_2O, O_2, and CO_2. Carbon monoxide, CO, is also known to degrade the photocathodes albeit at a lesser rate than these others [7.3]. However, the noble gasses, N_2, and H_2 with CH_4 (commonly present in UHV systems) in general do not chemically poison the photocathodes. While nothing intrinsic in the photoemission process itself degrades the QE, the operational lifetime never is as good as the dark lifetime, provided all other conditions are identical. The mechanisms for QE degradation while the beam is running include: a) the back-streaming of ions created by the electron beam ionizing the residual gas (ion back-bombardment); b) increased temperature of the photocathode due to laser illumination; c) beam losses and scraping in the gun's vicinity and the corresponding vacuum-degradation; and, d) back-streaming of chemically active species towards the photocathode surface. Common remedies to improve operational lifetime include off-center illumination of the photocathode to avoid ion back-bombardment of the active cathode area, and minimizing the active area (by deliberately reducing the QE outside the active region), thereby minimizing the production of an unwanted beam halo by the scattered light from the laser.

7.2.4 Summary of Photocathode Parameters

In Table **7.1**, we summarize the various relevant parameters for different semiconductor photocathode materials described in this chapter (after [7.4]). E_a is the electron affinity.

7.3 POSITIVE ELECTRON AFFINITY CATHODES: ALKALI-BASED PHOTOCATHODES

Some cathode materials actively pursued for photoinjectors are semiconductor cathodes with a positive electron affinity (PEA), such as cesium telluride and bi/multi-alkali antimonides. These cathodes have higher quantum efficiencies in the UV-Visible range of the radiation spectrum than metal cathodes (Figure **7.2**).

However, due to their sensitivity to contamination, they require UHV for fabrication, transfer, operation, and storage. We next describe the properties of these materials, their fabrication, transport into the photoemission gun, and performance.

Cathode Wavelength	**λ [nm] , E_{ph} [eV]**	**QE [%]**	**$E_a + E_{gap}$ [eV]**	**Thermal emittance $\left[\frac{\text{mm mrad}}{\text{mm rms}}\right]$**	
				Theory (Equ. 7.6)	**Experiment**
Cs_2Te	262, 4.73	~10	3.5	0.9	1.2 ± 0.1
Cs_3Sb	532, 2.33 473, 2.62 405, 3.06	~4 ~7 ~9	1.6 + 0.45	0.42 0.62 0.82	0.56 ± 0.03 0.66 ± 0.03 0.80 ± 0.04
Na_2KSb	330, 3.76	~10	1 + 1	1.07	N/A
Na_2KSb:Cs	390, 3.18	~20	1 + 0.55	1.03	N/A
K_2CsSb	532, 2.33 473, 2.62 405, 3.06	~4 ~11 ~25	1 + 1.1	0.38 0.58 0.80	0.56 ± 0.03 0.69 ± 0.03 0.87 ± 0.04
GaAs(Cs,F)	532, 2.33	~10	1.4 ± 0.1	0.77	0.47 ± 0.03
GaN(Cs)	260, 4.77	~15	3.4 ± 0.1	0.94	1.35 ± 0.11

Table 7.1. Commonly used high quantum efficiency photocathodes.

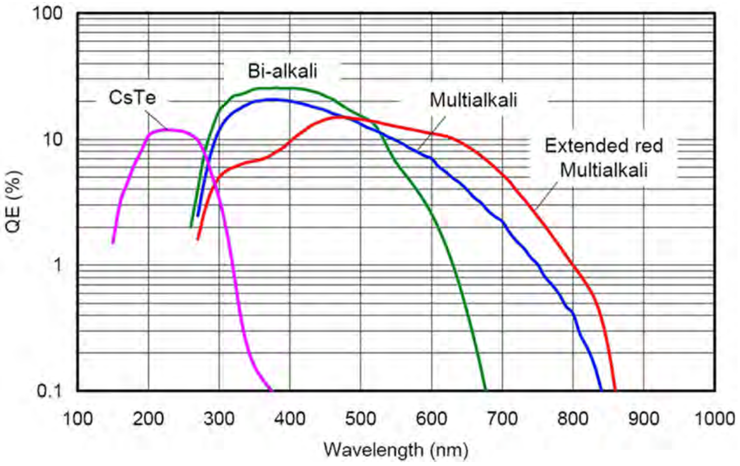

Figure 7.2. Typical spectral response for different types of photocathodes' materials. [7.5]

7.3.1 Materials Overview

Bi-alkali- and multi-alkali-photocathodes owe their development to the application of high sensitivity measurements of photons. Between the 1930s and '60s, considerable effort was made in developing and optimizing the performance of photosensitive materials, such as Cs_3Sb, K_2CsSb, Na_2KSb, and Na_2KSb:Cs. The fabrication process and the spectral response of these cathodes have been studied in depth [7.6]. However, due to the strong involvement of industry and the prospects of commercialization, much of the technical information is protected by intellectual property laws, and hence, details are not always readily available. Furthermore, since these cathodes were developed for detecting photons, *e.g.*, low current, low electric field applications, it was essential to reevaluate their performance in photoinjectors, wherein the peak current can be hundreds of amperes and the accelerating fields in excess of 100 MV m^{-1}.

The first successful use of these cathodes in an RF gun was in the APLE experiment in the early ’90s (the Boeing/Los Alamos Average Power Laser Experiment). By using a K_2CsSb photocathode, researchers demonstrated a world record average current (32 mA) for a photoinjector with a 25% duty cycle [7.7].

K_2CsSb is a stoichiometrically stable, p-type semiconductor with band gap energy of 1.0 eV [7.8], and an electron affinity of 1.1 eV. It has cubic crystal structure and high electron yield that is further increased by superficial oxidation. For these reasons, K_2CsSb is considered as a suitable candidate for photoinjector applications.

As with other semiconductor photocathode materials, cesium telluride was studied extensively as a solar-blind, UV sensitive detector. The stoichiometry of the cathode, investigated using X-ray photoemission spectroscopy (XPS) [7.9] was assigned as Cs_2Te. The crystal structure is not well established, but could be considered cubic, with polycrystalline surface. Earlier work by Powell *et al.* [7.10] established that this cathode is a p-type semiconductor with E_{gap} of 3.3 eV and E_a of 0.2 eV. Cesium telluride received particular attention because of its demonstrated insensitivity to contamination from O_2 and CO_2 compared with other alkaline photocathodes. This insensitivity makes this material valuable for guns whose vacuum cannot be held below the 10^{-7} Pa range, for example, normal conducting RF (NCRF) guns with a higher thermal load on the accelerating cavities [7.11]. Considerable effort was devoted to their preparation and characterization over the last 20 years. Even with the drawback of requiring UV photons, this is one of the most reliable high QE photocathode materials available to date.

7.3.2 Photocathode Fabrications Recipes

The realization of a good antimonide photocathode, whether involving a single alkali species or multiple ones, always starts with the deposition of a high purity Sb film onto a suitable substrate. Due to their initial application in photomultiplier devices, *e.g.*, photomultiplier tubes (PMTs), much of the literature on photocathodes focuses on the synthesis of photosensitive materials related to the deposition of very thin, semitransparent films on glasses. For these applications, the substrate usually is a transparent glass and the Sb film’s optimal thickness is determined experimentally by measuring the decline in the transmitted intensity of a white light source to about 85% of its initial value. In photoinjectors, the cathodes often are frontally illuminated, and thus, preferentially, an opaque photocathode is deposited on a suitable conducting substrate. For this reflection-mode photocathode, the thickness of the Sb layer typically does not need to exceed 20 nm. During the deposition process it usually is measured in-*situ* using a calibrated quartz-crystal microbalance. Similar considerations apply for Cs_2Te photocathodes.

7.3.2.1 Cs_3Sb

The synthesis of the cesium antimonide compound involves only a single source of alkaline metal and is rather simple. The differences in the recipes reported in literature are minimal. Once the substrate (the most common materials are molybdenum, stainless steel [7.12], and heavily doped silicon [7.13]) has been heated to about 160-150 ˚C, the Sb is evaporated until the film has the desired thickness. The substrate with the Sb film then is cooled down to ~130 ˚C, and exposed to Cs vapors. While Cs is reacting with Sb film to form the Cs3Sb compound, the photocurrent is measured. The Cs evaporation is stopped once the peak in quantum efficiency is observed (Figure **7.3**) [7.13].

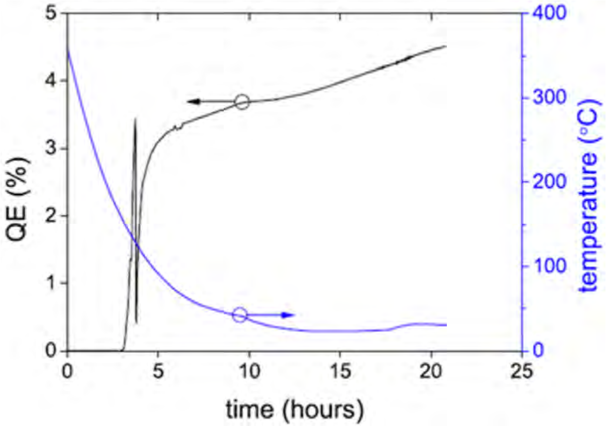

Figure 7.3. Quantum efficiency during the synthesis of a cesium antimonide photocathode. The peak in QE is reached at 3.5% as monitored by a 532 nm laser. A sudden drop in QE is due to an over-cesiation of the surface, from which it recovers after several hours. Each plot's axis is designated by the color and direction of the arrow. [Reprinted with permission from [7.13]. Copyright 2011, American Institute of Physics.]

The optimal thickness needed to maximize the light absorption, and hence the QE, from the photocathode layer at the desired wavelength is calculated using the complex index of refraction of Cs_3Sb and of the substrate [7.14] and considering that the Sb film with the correct stoichiometry should have a final thickness about 8X larger than that of the original Sb film [7.15]. Exposing Cs_3Sb to small amounts of oxygen (on the order of a fraction of a monolayer) can improve efficiency by an additional 50% [7.16].

7.3.2.2 Na_2KSb

While the literature contains only a few reports of Na_2KSb being used in operating photoinjectors [7.17], its satisfactory performances in PMT applications, especially at elevated temperatures up to 150 ˚C [7.18], makes it an interesting candidate as a material of choice for accelerators.

In general, a bi-alkali compound typically is grown through both substitution- and diffusion-chemical reactions. In the former, a stable binary alkali-antimonide compound is formed first. Exposure to the second alkali metal then partially replaces the first alkali species inside the crystal structure. The diffusion reaction uses a succession of depositions with the inter-diffusion of the alkali species required to form the final photocathode [7.19].

The standard recipe [7.6] for fabricating this photocathode again starts with the evaporation of a thin Sb film (usually a few nanometers) on a suitable substrate heated to about 160 ˚C. The second step is the growth of the K_3Sb photocathode (similar to the Cs_3Sb cathode): The Sb film is exposed to hot K vapor at ~160 ˚C until a peak on the photocurrent is reached. Then, the substrate is heated up to 220 ˚C and the substitution reaction with Na vapors is carried out until another peak in the photocurrent is observed.

Another approach consists of alternating many cycles of Sb deposition while keeping the substrate with the photocathode in a low pressure environment alternately rich in the vapors of alkali metals (K first, and Na after). Sb vapor is then introduced to react with the alkalis, leading to the growth of the photosensitive film [7.20].

The co-evaporation of both alkali metals and antimony was also undertaken in a dedicated molecular beam epitaxy (MBE) chamber, demonstrating a product with a QE comparable to commercial ones [7.21]. In this case, the temperature of the substrate is kept at 115 ˚C (lower than described above), and a mass spectrometer is used to control the flux of the chemical species during evaporation. The ratios of the mass signal on a mass spectrometer are kept equal to 1:10:15, respectively for Sb:Na:K. Tailoring the ultimate thickness of the photoemissive layer can minimize the reflection of the incident light to further improve the QE [7.19].

7.3.2.3 Na_2KSb: Cs

The synthesis of this multi-alkali photocathode is complex. The starting point is the growth of a high QE, Na_2KSb photocathode as described in the previous section. Thereafter, the cathode is left to cool down to about 160 ˚C and a very thin layer (a few nanometers) of Sb is grown on top. The Sb film is then allowed to react with Cs vapors to form a Cs_3Sb top layer. Growth can also be achieved in successive steps by alternating the deposition of Sb and alkali, [7.6] or by evaporating Sb in the presence of vapors of alkali metals [7.20]. The presence of the thin Cs_3Sb top layer is thought to lower the vacuum level of Na_2KSb close to, or even below the minima of the conduction band [7.22], [7.23], thereby allowing the extraction of a larger number of electrons from the photocathode, and extending its spectral sensitivity to the longer wavelengths up to about 1 μm.

7.3.2.4 K_2CsSb

The recipes used by different photoinjector laboratories generally are similar [7.24]–[7.28]. QEs of several percent routinely are achieved with ~ 530 nm radiation. Growth, similar to that of the previously described antimonide photocathodes, begins with few nanometers of Sb at a rate of 0.1-0.2 nm s^{-1} on a suitable substrate (molybdenum, stainless steel, and silicon are common choices) heated to temperatures between 100-180 ˚C. The Sb film then is left to cool to ~135 ˚C while being exposed to K vapors until the photocurrent reaches a maximum. Once the temperature drops below 130 ˚C, the exposure to Cs vapors begins. During this step, the cathode is left to cool down further, and the Cs flux is lowered to avoid its overexposure to Cs [7.29]. The exposure is stopped when the QE reaches the maximum value.

The temperature and the substrate material play a critical role in the formation of antimony layer. During evaporation at temperatures below 100 ˚C, the Sb layer on Mo and stainless-steel substrates appears patchy immediately after evaporation, but, with time, coalesces to form a more uniform, shinier surface. The rate of coalescence increases with temperature, taking up to a few minutes at room temperature to less than a few seconds at 100 ˚C. For substrates in this temperature range, the thickness of Sb measured using the crystal monitor and the SEM-EDX agree very well. Higher substrate temperatures result in lower sticking coefficient and correspondingly lower Sb thickness. For layer thickness of ~10 nm, SEM measurements show uniform film that conforms to the substrate, without any structure or crystal formation. The crystal structure of the initial Sb layer also seems to play a role in obtaining a high QE. Nakamura and collaborators demonstrated that the achievement of photocathode QEs as large as 40% in the visible range at 400 nm is related to the presence of well-defined Sb crystal peak on the X-ray diffraction spectra of the initial metal layer [7.30]. The role of the substrate is discussed in Section 7.3.3.2.

7.3.2.5 Cs_2Te

For a cesium telluride photocathode, the substrate (typically optically polished molybdenum) is held at 120 ˚C while several nanometers of Te (about 10 nm) are deposited at a rate of 1 nm per min. The film then is illuminated by UV light at 254 nm, and the Cs is evaporated at a similar rate while the photocurrent is monitored. When it reaches its maximum, the source and the substrate heater are turned off simultaneously [7.31]. Recent results [7.27] indicate that illumination with a longer wavelength (365 nm) supported the clearer identification of the QE peak (Figure **7.4**).

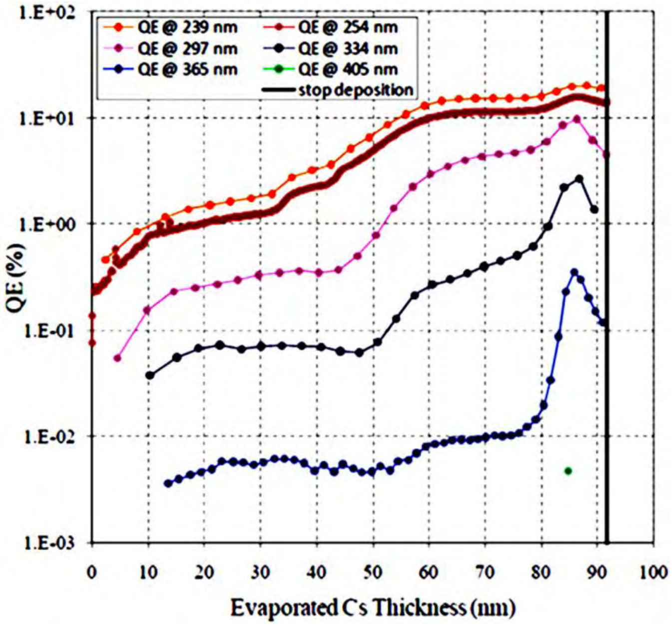

Figure 7.4. Quantum efficiency of a cesium telluride photocathode during Cs deposition. The photocurrent is measured at different wavelengths. By using photons at 365 nm, the peak on the QE is more evident. [[7.32]; Available under Creative Common Attribution 3.0 License (www.creativecommons.org/licenses/by/3.0/us/) at www.JACoW.org.]

Following this recipe typically ensures a QE of 10% at 264 nm [7.32]. The QE does not degrade if the cathode is stored in a UHV system with a base pressure of ~10^{-8} Pa. Auger spectroscopy performed during the deposition showed that the stoichiometry of the photosensitive materials gradually evolves during the reaction with Cs, and the peak of the sensitivity is reached when the ratio between Te and Cs is about 1:2 [7.33].

7.3.3 General Considerations for Cathode Fabrication

Requirements of the Deposition System

There are several common aspects in designing a deposition chamber for either Cs_2Te- or alkali-antimonide-cathodes. The mechanical design is affected heavily by the size of the photocathode (which determines the distance required between the substrate and the sources to achieve good uniformity), and the load-lock mechanism for transferring the cathodes from fabrication to the photoemission gun while maintaining the UHV condition for the cathode.

7.3.3.1 Metal Sources

Due to the strong reactivity of the chemicals (especially the alkali metals) involved in the growth of photocathodes, the choice of the sources and the design of evaporators deserve special attention. Also, the purity of the evaporated species can strongly influence the photocathode’s performance.

Sb: The source of high purity antimony either can be a metallic compound containing antimony, or high purity elemental antimony. Baumann *et al.* showed [7.34] that Sb from a metallic compound evaporates in small, possibly monatomic units of Sb, whereas that from elemental antimony appears as larger aggregates, such as Sb_4. For the simple thermal evaporation of commercial high purity (5N) Sb, the beads are placed in a tungsten- or tantalum-boat electrically heated up to a temperature where the equilibrium pressure of Sb under UHV is large enough to achieve a reasonable deposition rate. The latter depends on the size and distance of the substrate to the source. The temperature for evaporating Sb at a sufficient rate lies between 250-300 ˚C (the temperature for an equilibrium pressure of Sb at 10^{-6} Pa is 280 ˚C). Sb is evaporated mainly as tetramer (Sb_4) at these temperatures. If the photocathode recipe involves the co-deposition of Sb, it is convenient to use a cracker Knudsen cell that can break tetramers into dimers or even single atoms. Atomic Sb can improve reactivity with alkali metals.

Antimony also can be sputtered on to the substrate either in-*situ* or ex-*situ*. Substrates where antimony is layered ex-*situ*, the layer needs to be cleaned before evaporating the alkali metal, using techniques such as ion bombardment or heating. XPS measurements indicate that oxygen is the primary surface contaminant, most of which can be removed by heating the substrate to 400 ˚C. X-ray diffraction and SEM measurements of ex-*situ* sputtered Sb on Mo indicate that the Sb layer is amorphous for thicknesses up to ~ 7 nm, beyond which randomly oriented crystalline features were observed.

Tellurium also is evaporated from high purity beads (5N) but the needed temperature usually is lower than that required for Sb (the temperature for Te vapor pressure of 10^{-6} Pa is 155 ˚C). As with antimony, Te also sublimates as tetramer, so that using a cracker cell is recommended in MBE reactors. If the high vapor pressure of Te is a problem, an alternative approach is evaporating Te from a binary compound whose dissociation temperature is above the baking temperature. Indium telluride decomposes at 400 ˚C, above the bake temperature of most UHV systems, and its vapor pressure is under 10^{-6} Pa.

It is a good practice to degas the Sb/Te sources under vacuum before deposition to ensure the complete removal of surface contaminants that could be present either on the evaporation boat or the metallic beads.

Alkali: Different commercial sources are available for alkali metals: Alkali metal chromate powders, eutectic alloys, and pure metals.

Alkali-metal chromate powders mixed with a reducing agent are sold in small evaporators that must be resistively heated to a high temperature (can be more than 550 ˚C) before the chemical reaction yielding the metal vapor takes place. While the amount of alkali metals available in a single commercial dispenser is limited to a few milligrams each (usually suitable to generate a few photocathodes), they can be custom designed for larger capacity. These dispensers are not strongly reactive and can be exposed to air for assembling the source before placing them inside the vacuum chamber. For long term storage, the dispensers need to remain in a sealed, nitrogen filled container or be placed in a desiccator. Before starting the deposition, it is a good practice to degas these dispensers under vacuum by passing a current high enough to effectively heat them without starting the chemical reaction that generates alkali vapor. This current depends on the geometry and is usually specified by the manufacturer. During this process, the residual gas analyzer is used to monitor the partial pressure of the chemical species released (mainly CO, CO_2 and H_2O); degassing is complete once these are stabilized to partial pressures below 10^{-8} Pa. The presence of a getter (reducing agent Zr 84% Al 16%), however, usually precludes the complete release of the gasses from these dispensers. When designing the deposition chamber with short substrate-to-dispenser distances, the radiant heat load on the substrate during the high temperature heating of the dispenser should be taken into account. At source temperature in the range of 550 ˚C, the substrate temperature can exceed 100 ˚C inadvertently inducing unwanted changes in the specimen’s surface during deposition.

Dispensers based on intermetallic bismuth alloy are an alternative to the metal-chromate sources. They offer the advantage of providing larger quantities (for example, 25 mg of K and 100 mg of Cs in a 3 mm diameter container are available from Alvatec; and, higher quantities are available in larger diameter containers) of evaporable material with a much lower gas load while releasing the alkali species. Their main disadvantage is that these alloys still are strongly reactive with oxygen-containing species, and hence, are sold in small tubes filled with argon and sealed with an indium cap. Once the seal is broken, the sources cannot be exposed to air without becoming completely contaminated. The seal is broken by passing a small current (~ 4 A for a 3 mm diameter source) through the dispenser in vacuum, sufficient to heat and melt the indium. This step can be done towards the end of the bake cycle, when pumping is primarily through the turbo pump that is able to handle argon, and the partial pressure of contaminants is low. These dispensers also need to be heated to temperatures > 400 ˚C for sublimation of the alkali metals, thus, an eventual heat load on the substrate surface should be taken in account.

For mass producing large quantities of photocathodes (tens of cathodes without replacing the sources), using pure alkali metal sources should be considered. Alkali metals, such as K, Na, and Cs, can be purchased in sealed glass-ampoules filled with argon. Typical purities of 3N and amounts of material from few grams to many grams are obtained readily allowing the deposition of a very large number of specimens. The hazards of handling these ampoules should be taken into account considering their high reactivity with oxygen and water.

Commercial and custom designed MBE Knudsen cells can be used for loading the alkali metals in the deposition chamber. Since the evaporation temperature of these species is very low (~30 ˚C for Cs, ~65 ˚C for K, and ~140 ˚C for Na), care should be taken during the baking procedure of the UHV deposition chamber. The high capacity of these sources (up to many grams) and the expected long term stability (several hours for a fixed temperature) of the fluxes coming from MBE sources in principle will allow tens of deposition cycles depending on the source capacity before needing to refurbish the alkali metals, thereby supporting the optimization of growth parameters for achieving the best QE photocathodes. Another valuable aspect of these sources is their ability to produce uniform fluxes with a larger evaporation cone, making the alignment of the sources with the substrate less critical compared to conventional dispensers.

Eutectic alloys of alkali metals (NaK or CsK) can be used as an alternative; however, there are no publications documenting the results of using these alloys as sources of alkali metals for synthesizing bi-alkali photocathodes.

7.3.3.2 Substrate Requirements

The substrate for depositing a photocathode to be used in a photoinjector should incorporate the following abilities, *viz.*, to deliver high average replenishment currents (greater than milliamperes), and to conduct heat induced by the laser, which can be up to several tens of Watts. The glass substrates used in PMTs are unsuitable for this purpose due to their poor electrical- and thermal-conductivity. Stainless steel, molybdenum, or highly doped Si substrates, on the other hand, were shown to perform well.

The inertness of the substrate to the chemical species involved on the photocathode material growth should be considered to avoid diffusion at the boundary between the film and the substrate. Copper is a poor choice for the substrate, as it diffuses inside the photo-emitting layer [7.9], so explaining low efficiency of photocathodes grown on this material [7.35].

Assuring the cleanliness and flatness of the substrate is critical for photoinjectors. It is important to avoid unwanted contaminants on the substrate's surface that can diffuse inside the photosensitive layers or participate in the chemical reactions during growth. Oxygen-containing species, water vapors, CO, and CO_2 must be removed from the substrate surface before deposition. These molecules can be removed by thermal heating or ion sputtering, and their absence verified by surface analysis techniques, such as Auger spectroscopy. The most practical cleaning methods involve heating the substrate's surface above 400 ˚C [7.31]. For a Si substrate, the wafer is first rinsed in hydrofluoric acid to remove the native oxide layer, and then heated to 550 ˚C to remove the hydrogen passivation layer [7.36].

The flatness of the substrate plays an important role in determining one of the fundamental parameters of a photocathode, that is, its thermal emittance. Rough surfaces can cause considerably higher emittances of up to 60% [7.37]. Additionally, the chemical reactions leading to the formation of the photocathode seemingly are positively affected by good flatness in a substrate [7.35]. As the typical final thickness of the photoemitting layer is about 100 nm or less, the substrate's flatness is a key parameter, not only for low thermal emittance, but also to minimize the occurrence of field emission nucleated by surface defects.

The substrates for the Cs_2Te cathodes used in the TTF, PITZ, and FLASH injectors were formed from sintered or arc-cast Mo, machined to design specifications [7.31]. The plug is then chemically cleaned by buffered chemical polishing to remove the contaminants from machining. The surface roughness, a cause of dark current in a high electric field, is reduced by optical finishing. Figure **7.5** illustrates the improvement in the dark current with a polished substrate compared to a rough surface. To obtain an optical finish, the surface is successively polished with a set of diamond polishing compounds of decreasing grain size, the smallest being 0.1 μm. The measured reflectivity at 543 nm is 56.3%. The polished surface is then rinsed with acetone and ethanol in an ultrasonic cleaner, and then heated at 500 ˚C in UHV for approximately 30 min to reduce surface contaminants before fabricating the cathode.

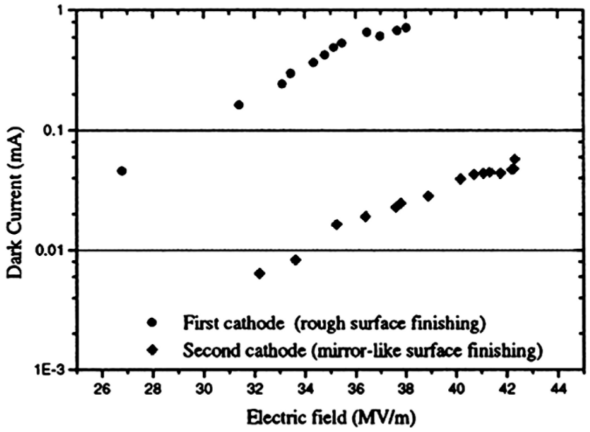

Figure 7.5. Effect of surface finish of the substrate of a Cs_2Te cathode on the dark current. [Reprinted from [7.38], with permission from Elsevier.]

7.3.3.3 Vacuum Chamber Requirements

The essential equipment for fabricating the cathode consists of a UHV chamber with high purity metals sources. The alkali sources and the cathodes themselves are very sensitive to contaminants (especially to water vapor, CO, and CO_2). The chamber should be able to reach UHV levels of $< 10^{-8}$ Pa. The system must be bakeable to ≥ 200 ˚C to completely remove water vapor. For vacuum isolation, all metal valves are preferable to reduce out-gassing, although metal bonnet valves are acceptable if there is a vacuum on both sides of the valve. Either magnetic- or bellow-translators are acceptable. The instantaneous increase in pressure during movement is higher for the latter than for the former. The system should have a sufficient number of ports to accommodate several viewports, electrical feedthroughs, and diagnostics. The viewports are used for observation and for irradiating the cathode to monitor the QE. The electrical feedthroughs are used for heating the sources and the substrate, connecting the thermocouple to measure relevant temperatures, and for measuring the current from the cathode to determine the QE. The electrical feedthroughs and connectors for heating should be chosen to minimize their heat load. The design and construction of the cathode preparation chamber should include the interface system for transporting the cathode from the preparation chamber to the gun. We discuss the details for the transport system later in this section.

7.3.3.4 Required Basic Instrumentation

The basic instrumentation needed to grow and perform initial characterization of the photocathode properties is the following:

- Metal Sources: Should provide uniform deposition profile with overlap from the other sources. The power supplies must be rated sufficiently high to heat the evaporators to the right temperature and ensure reliable evaporation. Equipping the sources with a thermocouple readout is optional, but useful for reproducing experimental results when the operational temperature of the sources is recorded. Again, it is preferable to isolate the sources to avoid their cross-contamination; their design should include a separate pumping system and isolation valve.
- Cathode (Substrate) Heater: The heater should be able to heat the cathode to higher temperatures (> 800 ˚C) when previous depositions must be removed from the substrate. A quartz heater is preferable since it reduces the accompanying gas load compared to tungsten filaments. A calibrated thermocouple to measure the temperature of the substrate is essential.
- Quartz Microbalance: This equipment is needed primarily to measure the thickness that is critical for forming stable stoichiometric compounds and growth rate of Sb or Te layers. The growth rate is measured either by placing the crystal monitor at the same location as the substrate and establishing the operating parameters to obtain this evaporation rate, or by positioning it at a different location and measuring the evaporation rate as the substrate is layered with Sb/Te. Since, in the latter approach, the monitor is not at the same place as the substrate, the thickness displayed by the microbalance must initially be calibrated against that on the substrate. Two different techniques can be used for calibration: 1) Measuring the optical transmission of a light beam of known wavelength through a transparent substrate while evaporating antimony; or, 2) taking the measurement externally. In the first technique, an optical beam of known power passes through the substrate before and after evaporation; thereafter, the thickness of Sb/Te is calculated *via* the formula $P_{out} = P_{in}e^{-\alpha t}$,where P_{in} and P_{out}, respectively, are the incident- and transmitted-power, α is the absorption coefficient, and t is the thickness of antimony/tellurium. Since the Sb aggregate from different antimony sources may differ, care must be taken to use the correct α in calculating the thickness. The sticking coefficient of the transparent substrate must be properly accounted for. In the second approach, the substrate with Sb/Te is removed from the vacuum chamber, and the signal (such as fluorescence, XRD) from elemental metal is measured against that of one with a calibrated thickness.
- Residual Gas Analyzer (RGA): The RGA is employed to monitor the composition of residual gas in the deposition chamber during all steps of the growth. It also is useful in indicating the onset of alkali-metal evaporation when the sources are heated. We recommend an RGA capable of detecting materials with a high atomic mass unit, such as Cs and Sb.

- Cold Finger: A cold finger aid in rapidly cooling the substrate and the photocathode after deposition, so that the alkali species do not evaporate from the finished photosensitive layers. Care must be taken to assure that it is not the coldest surface in the vacuum system because that would attract contaminants.
- Quartz Windows: These windows are used to illuminate the cathode's surface during the reaction with alkali metals to measure the photocurrent and QE while evaporating different alkali species. Quartz is essential when using the UV light for Cs_2Te growth and for spectral response measurements. Mechanical shutters to these windows reduce any unwanted metal coating of their surfaces.
- Light Source and Lock-In Amplifier: A D_2- or Hg-lamp with a monochromator is useful for obtaining the cathode's spectral response. Ideally, the light source is equipped with a chopper so that a lock-in amplifier can be used to measure the photocurrent. The lock-in amplifier also removes the background DC current generated by stray photons of different wavelengths entering the UHV chamber.
- Vacuum Pumps and Gauges: These should be able to handle the range of pressure and the atomic species during evaporation. We note that for a given vacuum level, the base current of an ion pump may increase due to the metal coating of its electrodes, engendering a corresponding change in resistance. Hence, using ion pump current to extrapolate the vacuum level should accompany frequent calibration.

There are two possible source-substrate designs: All sources pointing to the substrate center, with substrate held in one position (Figure **7.6(b)**), or a substrate that can be translated in front of each of the sources in succession (Figure **7.6(a)**). Each design has its advantages and disadvantages. Figure **7.6(b)**, both the substrate and the crystal monitor are held in one position and the evaporation is achieved either by heating one source at a time or in parallel for co-deposition. The geometry of the sources and the substrate must be carefully designed to maximize the overlapping region of evaporation cones as shown in Figure **7.6(b)** and to minimize the evaporation time. The major disadvantage is non-uniformity of the cathode over the entire evaporated area. In the latter design, the substrate is positioned normal to each source, resulting in a better uniformity of the film. However, both the substrate and the crystal monitor should be translated when changing the sources, so complicating the design of the substrate holder. Both designs should allow the sources to be retracted away from the deposition chamber when not in use.

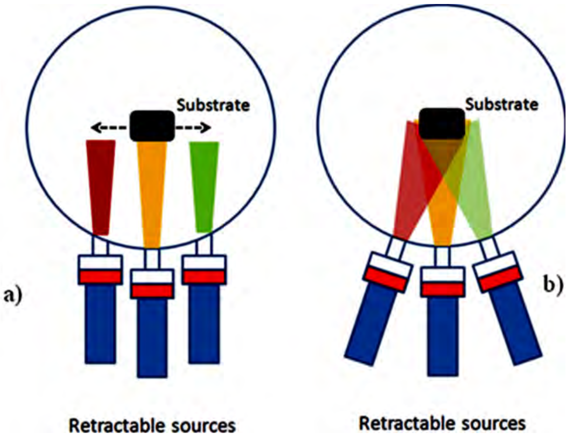

Figure 7.6. Two possible configurations for growing alkali-based photocathodes. (a): The substrate is shifted frontally to each source for a sequential deposition of different elements. (b): The sources are pointing towards the center of the substrate with the evaporating fluxes overlapping over its surface.

The current emitted from the cathode can be measured either from the cathode, or collected by a low voltage bias anode close to the substrate between the electrodes to overcome space charge effects. A QE map of the cathode area is obtained by irradiating light at a single wavelength and scanning a small laser spot on the cathode while measuring the QE. Figure **7.7** shows examples of such scans.

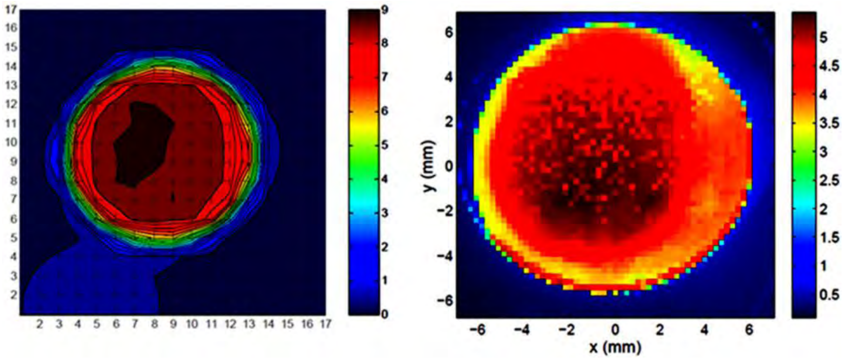

Figure 7.7. Examples of 2-D scans to measure the QE uniformity: A Cs_2Te photocathode at 254 nm (left), and a Cs_3Sb photocathode at 532 nm. [Reproduced from [7.39]] [Reprinted with permission from [7.13]. Copyright 2011, American Institute of Physics.]

Figure **7.8** is a schematic of an UHV growth chamber with the basic instruments needed to synthesize a semiconductor, high QE photocathodes. Therein, the main chamber is equipped with an RGA for monitoring the constituent gases, and gauges for measuring the overall vacuum level; it has two windows for light transmission (input and output), a quartz microbalance crystal to measure deposition rates and thicknesses of evaporated layers, and the substrate holder equipped with a heater and a cold finger. Several vacuum ports allow the connection of a pumping system (a combination of ion pump, titanium sublimation pump, and NEG modules) that can reach a pressure below 10^{-8} Pa. The metal sources facing the cathode surface can be retracted and isolated from the main chamber *via* vacuum gate valves to prevent cross-contamination. Another valve allows insertion and removal of the cathode substrate without breaking the vacuum of the main chamber.

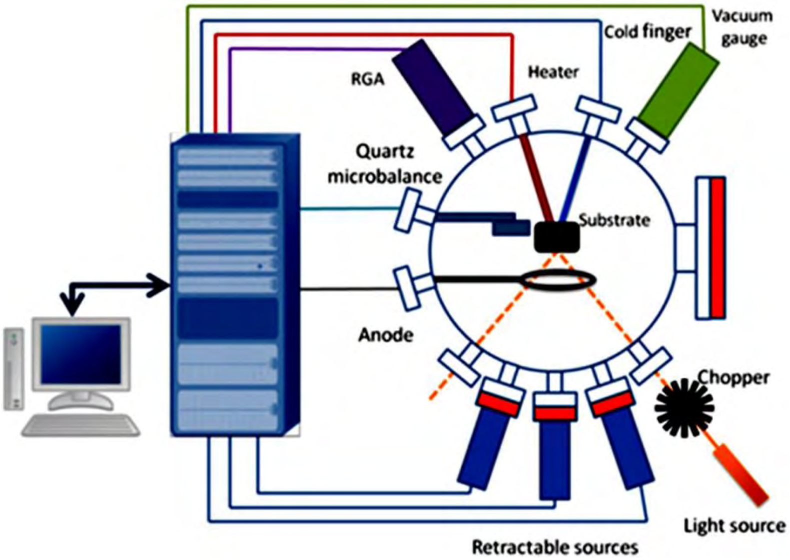

Figure 7.8. Schematics showing a typical UHV chamber set-up for growing alkali-based photocathodes. All instrumentation is interfaced with a personal computer for setting the experimental parameters for the growth and recording the data for each deposition. Red rectangles indicate the gate valves used for sealing the metal sources to avoid cross-contamination and for loading the photocathode substrate. For simplicity, the pumping systems for both the UHV chamber and individual source assemblies are omitted.

When the cathode in the gun must be replaced often, it is convenient to design a suitable vacuum suitcase and a photocathode storage chamber that can accommodate multiple substrates simultaneously. The suitcase is used to transfer the cathode between the storage or the deposition chamber and the photoinjector under UHV conditions. With such a set-up, Cs_2Te cathodes are fabricated in LASA, Milan, Italy, and routinely transported to injectors in TTF, PITZ, and FLASH. Similarly, the K_2CsSb cathode was fabricated at BNL and tested in a DC gun at JLab. It is desirable to have the ability to monitor the QE of the photocathodes during and after their transport to the photoinjector. We have used magnetically coupled translators successfully for moving the substrates back and forth from the vacuum suitcase and the cathode to and from the injector. The following are the essential components of the transfer system (Figure **7.9**):

- A UHV transfer chamber with translators to move the cathode from the fabrication chamber to the injector
- a pumping section to maintain vacuum during transport
- an intermediate section with two valves and pumping station connecting the fabrication chamber/injector. The temperature of the cathode must carefully be maintained close to room temperature when this intermediate section is baked and pumped before opening the valves to transfer the cathode.

7.3.4 Photocathode Performance

7.3.4.1 Quantum Efficiency and High Current

Several institutions have fabricated Cs_2Te cathodes and transported them successfully the RF injector, for example, CLIC [7.40], TTF [7.41]**,** FLASH [7.42], PITZ [7.43], and Los Alamos [7.44]. In the injector, the cathode must meet additional requirements, such as delivering a large photocharge at low emittance, reliably and reproducibly with very low dark current. The publication describes how Cs_2Te cathodes with an average QE of 9% at 264 nm are reproducibly fabricated at LASA, Milan. This average QE fell to ~2.5% upon transport to, and use in the gun at DESY. The initial dark current from these cathodes depends strongly on the cathode's substrate and the accelerating field in the cavity [7.44]. During operation in the gun, the dark current from the cathode also increases, probably due to cavity conditioning. Furthermore, the gun's vacuum also degrades during high current operation resulting in additional exposure of the cathode to gas and its subsequent degradation of QE and increased the dark current [7.42]. Single pulse charges of up to 50 nC without any saturation effects were delivered with this cathode material. Pulse train lengths of 30 μs with a repetition rate of 1 MHz and a charge per bunch of 1-8 nC were produced routinely with the Cs_2Te cathode at FLASH; furthermore, the train length was extended to 300 μs. The operational life time of the cathode, defined as the time at which the QE drops to 0.5%, is between 100-200 days; hence, a vacuum suitcase with two or three cathodes can service the injector for over a year.

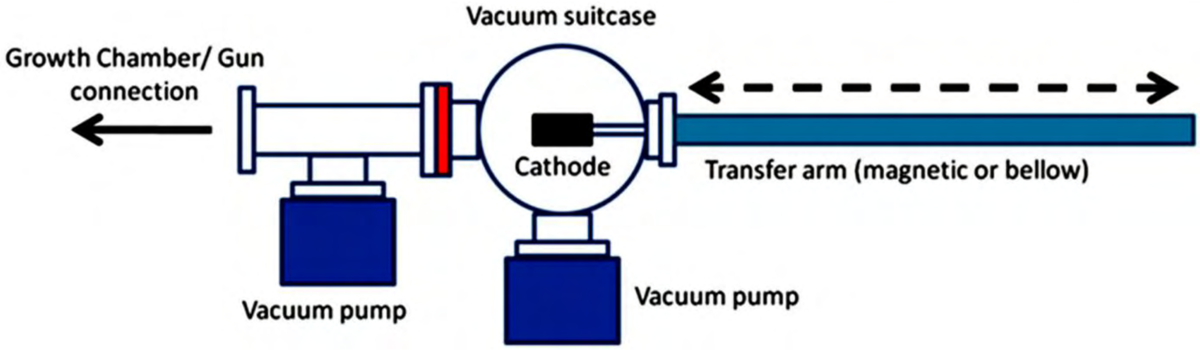

Figure 7.9. Schematics of a vacuum suitcase for transferring photocathodes from the deposition chamber to the electron gun. The red rectangle indicates the gate valves used to seal and keep the photocathode under UHV during transport.

Similarly, K_2CsSb cathodes were tested in both NCRF [7.7], [7.24] and DC guns [7.45]. They achieved QEs in excess of 14% at 532 nm, average current of 32 mA [7.24], and current densities exceeding 160 mA mm^{-2} [7.45].

Beam brightness is defined as a ratio between the beam's current and its emittance (either in 2-D-, 4-D-, or 6-D-phase space). Accordingly, the way to increase the beam's brightness is by raising its current, lowering the transverse emittance, and/or the pulse duration-energy spread. In addition to the QE, other fundamentals characteristics of a photocathode operating in a photoinjector are its thermal emittance, response time, and lifetime.

7.3.4.2 Thermal Emittance

A simple relationship can be used to roughly estimate thermal emittance [7.4]

$$\epsilon_{nx,th} = \sigma_x \sqrt{\frac{\mathrm{MTE}}{3m_0c^2}}; \text{ where MTE} = E_{ph} - (E_{gap} + \eta) + \phi_{Schottky} \tag{7.7}$$

Here σ_x is the laser rms spot size, MTE is the mean transverse energy of photoemitted electrons, m_0c^2 is the electron rest energy, $E_{gap} + \eta$ is photoemission threshold energy, given by the sum of E_{gap} and electron affinity, η. Thus, $E_{ph} - (E_{gap} + \eta)$ represents the maximum excess kinetic energy imparted to electrons by the photons. $\phi_{Schottky}$ is the effective reduction in work function when strong external electric field is present.

The Schottky lowering of the work function is determined by the effective electric field, E, at the photocathode's surface

$$\phi_{Schottky} = \sqrt{\frac{e^2E}{4\pi\varepsilon_0}} \tag{7.8}$$

or, in practical units

$$\phi_{Schottky}\,[\mathrm{eV}] = 0.0379\sqrt{E\left[\frac{\mathrm{MV}}{\mathrm{m}}\right]} \tag{7.9}$$

As the physics of photoemission processes is complex, the Equ. 7.7 can only be used as a rough guide. Even though the photocathode materials based on alkali-antimonides and tellurides have been known for decades, only recently have staff at different laboratories determined MTE values experimentally. Some of these results are shown in Figure **7.10** and Figure **7.11**.

The former depicts the very good agreement with Equ. 7.7 for CsK_2Sb. The latter illustrates the dependence of the thermal emittance on the intensity of the extracting field: at the higher fields, for a given photon energy, thermal emittance increases because of the reduction in work function due to the Schottky effect, Equ. 7.8. Table **7.1** in Section 7.2.4 compares the data with Equ. 7.7, indicating a fair agreement between theory and experiment for alkali-based materials. Normalized emittance of 0.37 µm $mm\text{-}rms^{-1}$ has been measured from a K_2CsSb cathode held at ~2 MV m^{-1} and irradiated by 534 nm optical beam by [7.26]. Similar results have been obtained for Cs_2Te cathodes as well. [7.44]

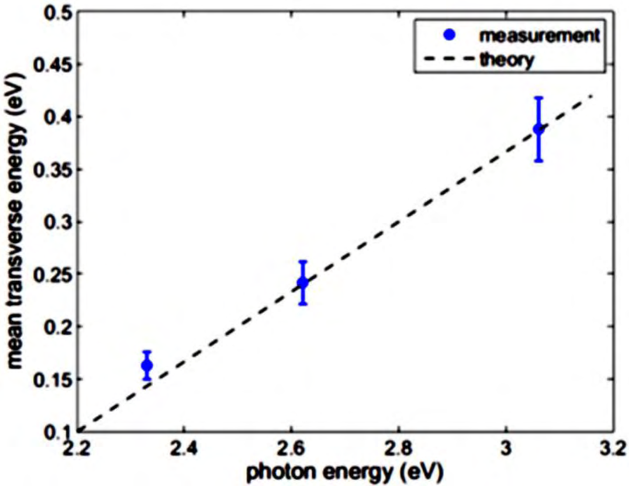

Figure 7.10. Comparison between the experimental values obtained for the MTE of electrons emitted by a K_2CsSb photocathode at different wavelengths and the model prediction obtained using Equ. 7.7. [Reprinted with permission from [7.25]. Copyright 2011, American Institute of Physics.]

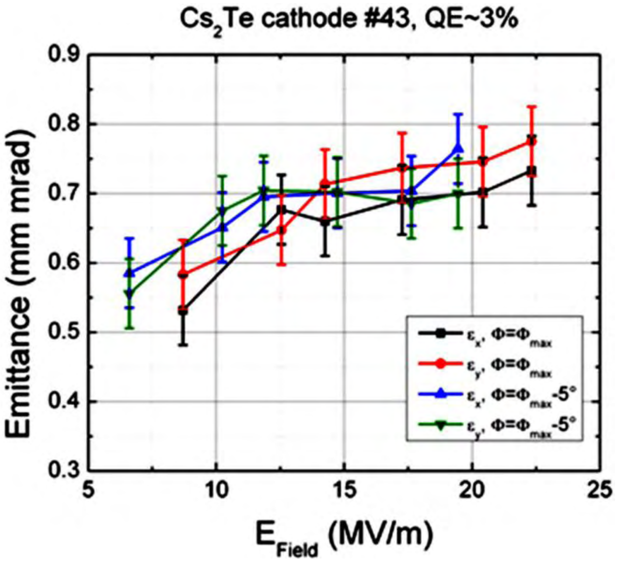

Figure 7.11. Thermal emittance measurement from a Cs_2Te photocathode for different values of the extraction electric field. Thermal emittance increases at higher electric fields due to the Schottky effect. [[7.44]; Adapted under Creative Common Attribution 3.0 License (www.creativecommons.org/licenses/by/3.0/us/) at www.JACoW.org.]

7.3.4.3 Response Time

A photocathode response time of < 1 ps is desirable for most photoinjector applications so that the electron beam's temporal profile reflects the laser's temporal shape. A much longer response time (tens of picoseconds) usually is unacceptable unless a complex RF bunching and chopping system is being employed. Alkali-based photocathodes in the form of thin films are used in modern streak camera devices, demonstrating a very fast response time (a time resolution of 200 fs is commercially available) [7.46], [7.47]. Recent measurements carried out in photoinjectors by using an RF deflecting cavity confirmed that the response time from Cs_2Te and Cs_3Sb (Figure **7.12**) is on the picoseconds scale, or shorter [7.13], [7.48].

7.3.4.4 Lifetime

Lifetime is a critical parameter for a photocathode used for generating the beam in modern photoinjectors. For alkali-antimonide materials, the factor limiting the photocathode's dark lifetime essentially is poisoning, caused by the oxidizing species in the residual gases inside the gun chamber. Indeed, poor vacuum conditions during the operation of the Boeing RF gun restricted the operation of a CsK_2Sb photocathode to about several hours due to reactions with water vapors inadvertently present in that RF gun's vacuum (Figure **7.13**) [7.24].

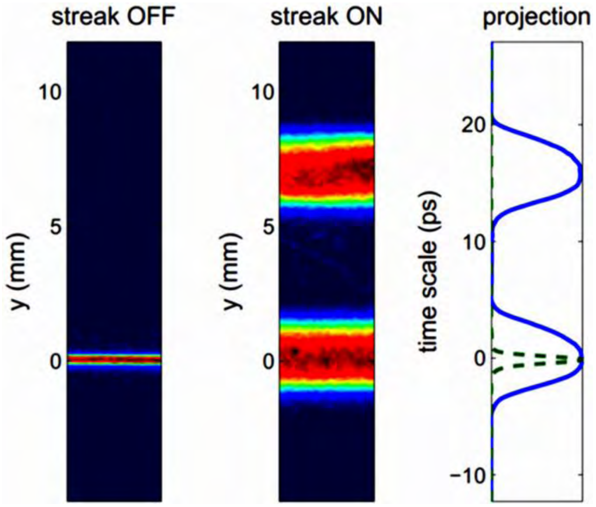

Figure 7.12. Example of a measurement to determine the response time using an RF deflecting cavity. Electron beam generated by two laser pulses with a duration of about 1 ps rms and separated by 16 ps (green dashed line on the right plot) are vertically deflected by the RF cavity. The temporal profile is obtained using a view screen, and the upper estimate of the response time is obtained (additional causes contributing to the width are the RF laser synchronization, or fluctuations in arrival time). [Reprinted with permission from [7.13]. Copyright 2011, American Institute of Physics.]

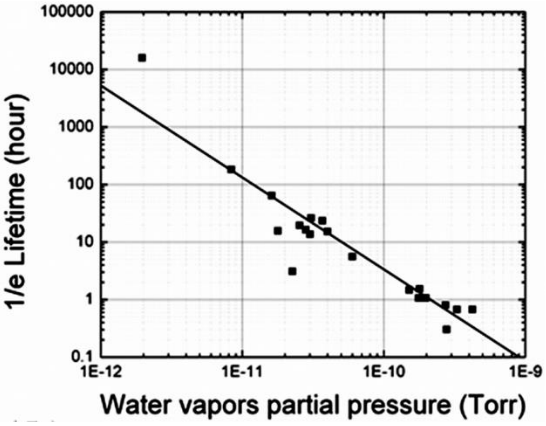

Figure 7.13. Plot of experimental data of 1/*e* lifetime of K_2CsSb photocathode operating at different levels of water vapor partial pressures (reproduced from). Recent results indicate possibly longer lifetimes [7.26]. [Adapted from [7.24], with permission from Elsevier]

Recent studies indicate that the QE decays from 6% to ~1.5% over 20 hr in 10^{-10} Pa partial pressure of water when illuminated with 532 nm light [7.25].

The same poisoning effect due to poor vacuum might have contributed to the degradation of the QE of a Na_2KSb photocathode operated at 10^{-6} Pa inside a RF gun at Tokyo University, even though the authors attributed the decay to the presence of high intensity electric fields, up to 100 MV m^{-1} [7.49]. In a more favorable vacuum environment, K_2CsSb cathodes are very stable and have demonstrated the ability to deliver high average beam currents for long periods. For example, the DC gun of the ERL photoinjector prototype operated at Cornell University with a base vacuum level of ~10^{-10} Pa used a K_2CsSb photocathode to deliver an average current of 20 mA and current density of 10 mA mm^{-2} for 8 hr, with only a slight decrease in the QE (Figure **7.14**) [7.36].

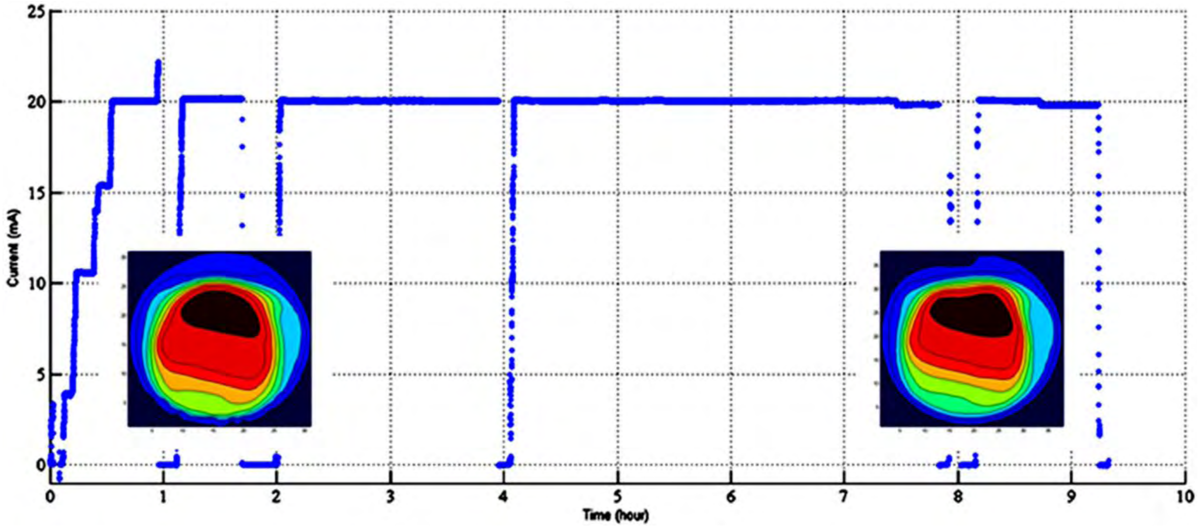

Figure 7.14. The photocurrent extracted from a K_2CsSb photocathode from the DC gun of the ERL prototype at Cornell University. A 20 mA average current was delivered for 8 hr. 2-D scans of the photocathode's QE show negligible degradation after the run (compare the QE maps before the run, on the left, and after the run, on the right). [Adapted figures with permission from [7.50]. Copyright 2011 by the American Physical Society]

Cs_2Te photocathodes are less sensitive than alkali-antimonide ones to poisoning by harmful residual gases [7.11]. Figure **7.15** plots the change in the QE of the former for typical residual gases found in a UHV system. Cs_2Te photocathodes have demonstrated operational lifetimes for up to four months (Figure **7.16**) [7.50].

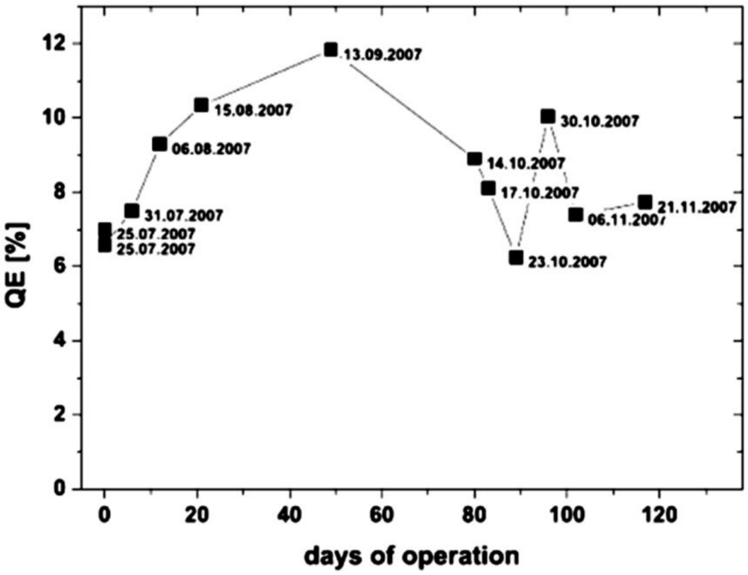

Figure 7.15. QE measurement of a Cs_2Te photocathode operated in a photoinjector showing an in-gun lifetime of about 4 months. [[7.51]; Available under Creative Common Attribution 3.0 License (www.creativecommons.org/licenses/by/3.0/us/) at www.JACoW.org.]

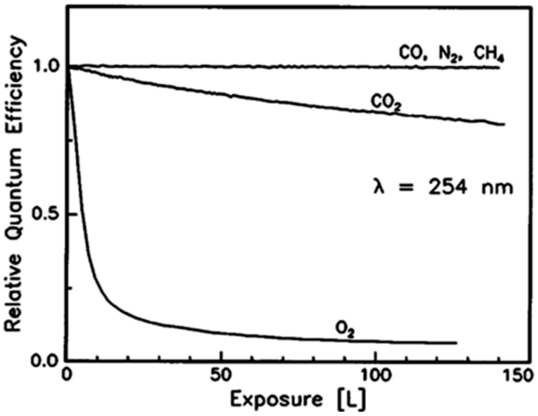

Figure 7.16. Sensitivity of Cs_2Te cathode to contaminants. [Reprinted with permission from [7.9]. Copyright 2011, American Institute of Physics]

7.4 NEGATIVE ELECTRON AFFINITY CATHODES: III-V PHOTOCATHODES

7.4.1 Overview

III-V semiconductor materials (GaAs, in particular) have been operating in accelerators as a photocathode material in photoinjectors since about the last quarter of the 20th century. Initial interest in GaAs mainly was stimulated by polarized electron beam production (Chapter 8). To maximize the electrons' polarization, the laser's photon energy necessarily must be near the band gap, with modest QE (of ~0.1-1%). Apart from generating polarized beams, III-V semiconductors activated to negative electron affinity (NEA) (Figure **7.1**) possess several characteristics suitable for high average current photoinjectors. Among their advantages are very high quantum efficiencies (10-20% is typical, with reported values higher than 50%), prompt response time (< 1 ps) when excited with photon energies much larger than the band gap energy, very low thermal emittance, and mean transverse energy that is essential for low emittance photoinjectors. Furthermore, the quick activation with cesium on samples with atomically clean surfaces is another advantage; in many cases, degraded photocathodes readily are restored by depositing a monolayer of cesium either with or without high temperature treatment. The main drawback of these families of photocathodes lies in their high sensitivity to contaminants and stringent vacuum requirements (10^{-9} Pa or better).

The material discussed herein covers high quantum efficiency, III-V semiconductor photocathodes suitable for high current applications. Much of the technology for the photocathode preparation is similar to that of the polarized sources (Chapter 8); therefore, the emphasis is on peculiarities specific to high QE photocathodes used in high current, low emittance photoinjectors. Chapter 4: DC/RF Injectors is a complementary chapter in this book covering technology aspects related to the performance, and preparation of GaAs photocathodes, and their transfer.

7.4.2 Properties and Preparation

III-V semiconductors, suitable as high efficiency photocathodes, are direct band gap materials that rely on their good photoemission properties *via* NEA, a condition established at their surface by the deposition of a single monolayer of very electropositive alkali metal (cesium), as shown in Figure **7.17**. The term direct band gap signifies that the valence band maximum (VBM) is aligned directly below the conduction band minimum (CBM) in momentum-energy band gap diagrams. The implication therein is that the absorption of a photon by an electron in the valence band and its subsequent promotion to the conduction band occurs as a single-step process. This transfer is depicted by a vertical line in diagrams of momentum-energy band gap because the photon carries a negligibly small momentum compared with much heavier electrons and holes in semiconductor. Those transitions, known as vertical- or direct-transitions, occur without needing an additional momentum transfer from the crystal lattice's vibrations, as is required for indirect band gap materials, where VBM and CBM have different momenta in the band-energy diagram. Consequently, the probability of optically promoted transitions across the band gap is much higher in direct band gap semiconductors, leading to their high quantum efficiency.

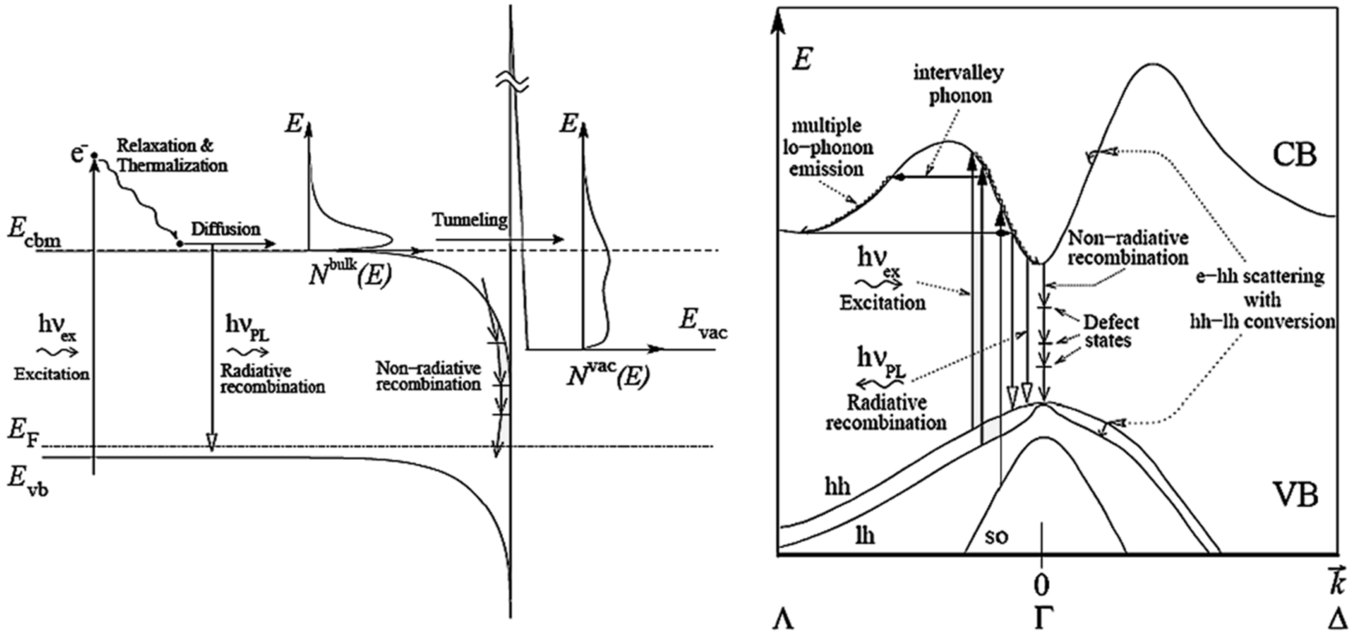

Figure 7.17. Energy versus electron lattice momentum (left), and energy level structure near the surface (right). *CB* – conduction band; VB – valence band; E_F – Fermi level; *hh*, *lh*, *so*, and *lo* represent heavy hole, light hole, split off energy bands, and longitudinal optical (phonons), respectively. ν_{ex} is the excitation frequency and ν_{PL} is the photoluminescence frequency. [7.52]

There are excellent reviews of this class of materials, including a book by Bell [7.53], and a chapter by Escher [7.54]. There are several different materials in this category, with much interest traditionally devoted to IR sensitive devices (*e.g.*, InAs and related tertiary compounds). We discuss two materials as practical photocathodes for photoinjectors: GaAs and GaN. The first was used extensively in photoinjectors operating at high current, and has a conveniently large response in the visible range with the band gap of 1.42 eV at room temperature. On the other hand, GaN is a newer material for photoinjectors with a wide band gap of about 3.4 eV, and there is limited experience of its use. Finally, there is considerable flexibility in growing new high quality semiconductor structures with the desired properties for accelerators. We summarize some interesting developments employing tertiary structures (*e.g.*, AlGaAs) and other advanced ones for high QE unpolarized photocathodes in photoinjectors.

Achieving NEA (Figure **7.1** and Figure **7.14**) is central to a good QE of III-V photoemitters. Pure crystals with atomically clean surfaces are poor photoemitters with a work function of about 4 eV. Two main mechanisms establish the NEA: 1) A strong p-doping, inducing band bending near the surface; and, 2) through the donation of an electron toward the bulk by strongly electropositive alkali metal (cesium being the commonest although Li, Na, K, and Rb also have been used). Additional exposure to an oxidizing agent and cesium forms an even stronger dipole on GaAs, whereas GaN can be activated to NEA with only Cs. On the atomic level, NEA is understood as electron emission assisted by strong dipole fields formed preferentially so that a large negative electric field points towards the surface, accelerating electrons in the opposite direction. Table **7.2** shows some basic material properties for two of the III-V semiconductors detailed in this chapter.

Material	**GaAs**	**GaN**
Structure	Zinc Blende	Zinc Blende or Wurtzite
Energy gap (@ 300 K) [eV]	1.42 (direct)	3.2 or 3.44
Electron effective mass [Γ]	$0.067m_0$	$0.13m_0$ or $0.20m_0$
Melting point [K]	1511	2773
Thermal conductivity (@ 300 K) $\left[\frac{\text{W}}{\text{cm K}}\right]$	0.55	2.3
Density $\left[\frac{\text{g}}{\text{cm}^3}\right]$	5.32	6.15

Table 7.2. Some basic material properties of GaAs and GaN [7.55].

7.4.2.1 GaAs

Preparing a bulk GaAs photocathode starts with obtaining a high quality crystal. Different atomic orientations can be used: (100) and (110) are typical, with (110) orientation cleaving easily. Manufacturers offer specific crystalline orientations (epitaxial-ready surface). A small angle to a specific atomic plane is attainable without any apparent detrimental effect on the photocathode's performance. Doping levels are important, preferably with high p-doping to ensure both the wafer's band bending and good conductivity. For example, common dopant densities (typically Zn) for high QE, unpolarized GaAs photocathodes used in high current applications is $0.6\text{-}2\times10^{19}$ cm^{-3} with a low resistivity of 5-7 mΩ cm.

The surface of the semiconductor wafer is critical; it must be atomically clean before activation and, ideally, atomically flat. The preparation includes chemical cleaning ex-*situ* and heat- and hydrogen-cleaning in-*situ*. Table **7.3** gives typical steps used by two groups, one at Stanford University, and the other at Cornell University [7.56], [7.57]. No uniform procedure exists and the details of wafer preparation vary.

While the wet chemistry effectively removes carbon-containing impurities, oxygen and oxides forming on the surface of GaAs play a critical role both in achieving the high QE and assuring a smooth surface. A surface free from carbon contaminants, but having oxides does not lend itself to NEA activation. A layer of natural oxides forms readily in the atmosphere. To minimize exposure of the GaAs surface to oxygen, the Stanford group undertakes their wet chemistry in an Ar atmosphere. Some groups found that hydrogen cleaning effectively removes both oxygen and carbon once the semiconductor wafer is in vacuum. High temperature cleaning is an essential practice adopted by all groups employing GaAs; its main benefit is in breaking oxides. The exact value of the temperature is a critical parameter. Previous wet chemistry treatment in Ar atmosphere, effective at removing oxygen, allows a comparatively low temperature treatment (≤ 500 ˚C). First, the most volatile oxide AsO is desorbed at a temperature as low as 150 ˚C [7.58]. The more stable As-oxide, As_2O_3, breaks down at about 300 ˚C forming Ga_2O_3. Both Ga_2O_3 and GaO_2 are much more stable, requiring temperatures in excess of 500 ˚C to destabilize them. Gallium oxides are removed effectively at 580 ˚C; however, both Ga and As start to evaporate at that point. Also, 620 ˚C is known as the temperature of onset of non-congruent evaporation, *i.e.*, As starts leaving the surface preferentially, leaving a Ga-rich surface. Beyond that temperature, the structure of GaAs crystal is compromised entailing the deteriorated performance of the photocathode. Thus, high quantum efficiency photocathodes are routinely produced at Cornell University (15% at 532 nm) under heat treatment at 620 ˚C for 1-2 hours with no hydrogen cleaning. However, surface roughness increases substantially at these high temperatures [7.58]. Figure **7.18** shows the surface rms roughness as a function of heat cleaning temperature, along with depictions of a sample's surface [7.58]. Such a rough surface, while acceptable for photoinjectors that do not require the smallest emittances, are suboptimal for applications wherein emittance is a critical parameter [7.60].

Stanford [7.56]	**Cornell [7.57]**
Wet chemistry: H_2SO_4:H_2O_2:H_2O (4:1:100) for 2 min HCl:H_2O (1:3) for 2 min or H_2SO_4:H_2O (1:1) for 30 sec	Wet chemistry: Acetone and trichloroethylene cleaning H_2SO_4:H_2O_2:H_2O (20:1:1) for 1 min
Chemistry is done in Ar chamber connected to a load-lock system	Anodization and NH_4OH treatment to limit QE active area; transported in air
Heated to 500 ˚C	Optional atomic hydrogen cleaning
Cs + O_2 co-deposition	Heat cleaning at ≤ 620 ˚C
	Cs + NF_3 "yo-yo" process

Table 7.3. Cleaning and preparation steps for GaAs photocathodes [7.56], [7.57].

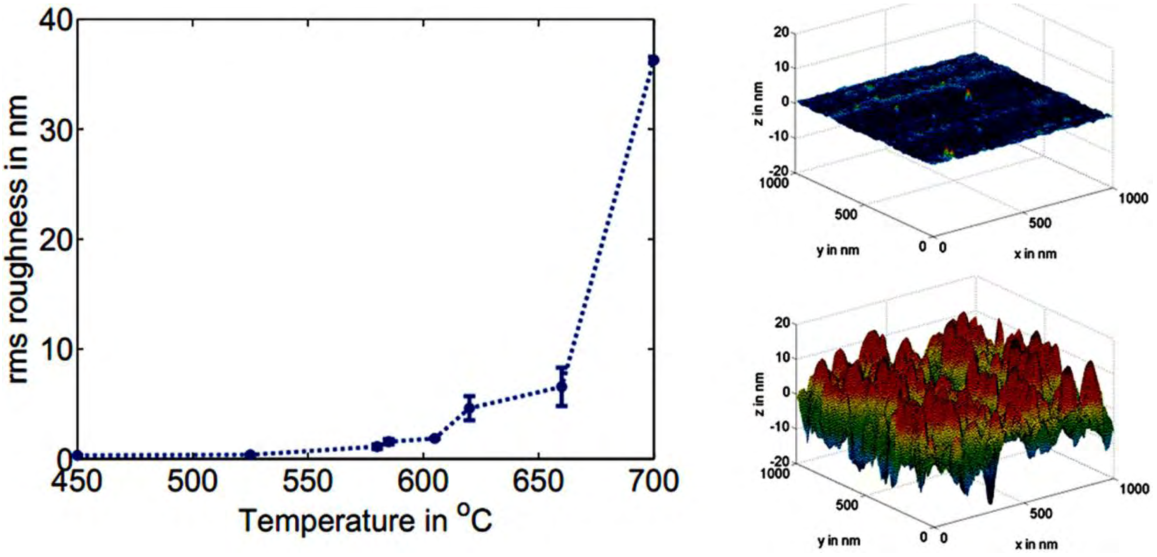

Figure 7.18. Surface roughness versus temperature for heat treatment of GaAs (left). Examples of AFM measurements on untreated GaAs (upper right) and after the heat treatment (lower right). [[1.1][2.1][4.1][5.1][6.1][7.1]; Available under Creative Common Attribution 3.0 License (www.creativecommons.org/licenses/by/3.0/us/) at www.JACoW.org.] [Reprinted with permission from [7.60]. Copyright 2011, American Institute of Physics]

Once a clean, oxide-free surface is established, the cathode is activated to NEA. QE is measured continuously during this activation process. Initially, about a monolayer of Cs is deposited resulting in an initial increase of QE (2-5% at 532 nm wavelength). As Cs is deposited, the QE rises to a peak and then starts to drop. Only the deposition of Cs continues until the QE reaches about half the value of the first peak. At that point, an oxidizing agent is used further to increase QE. NF_3 or O_2 are commonly used as the oxidizing agent, producing similar results. NF_3 reacts with Cs forming CsF at the surface, with nitrogen escaping the surface. However, detailed studies of the activation layer [7.61] revealed that the actual composition of the layer was complex, with N embedded in it. Two different techniques are used with good success: "Yo-yo" (Figure **7.19** left) and co-evaporation (Figure **7.19** Right). Using the "yo-yo" technique, the exposure of NF_3/O_2 and Cs is alternated, whereas for co-evaporation, it is held at a constant rate until the QE reaches its maximum. Studies indicate that electron affinity is close to 0 eV for only Cs and becomes -0.1 eV for a fully activated photocathode.

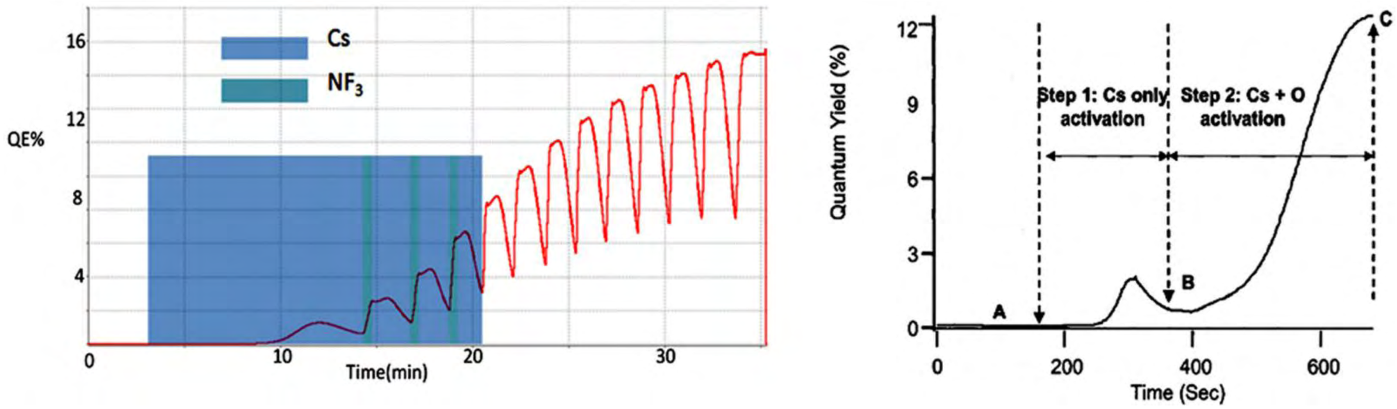

Figure 7.19. "Yo-yo" activation with Cs and NF_3 (left, the activation pattern shown persists throughout the entire procedure), and co-evaporation of Cs and O_2 (right). [7.56]

The typical dark lifetime of GaAs is on the order of days (even though CEBAF demonstrated the essentially infinite dark lifetime for their polarized photocathodes). A practical solution for rejuvenating the photocathode is reactivation with Cs that routinely restores the QE to 5% or higher (at 532 nm). High temperature cleaning is a reliable method to restore the QE of GaAs to its original performance, except after particularly heavy damages from ion back-bombardment and sputtering.

Because the vacuum requirements for GaAs are so stringent (vacuum of $\leq 10^{-9}$ Pa with RGA spectra free from water, oxygen, and carbon dioxide), transfer of this photocathode has not accomplished without affecting its sensitive activation layer. Presently, all guns operating with GaAs either have a preparation chamber attached to them (the preferred solution), or are activated inside the gun.

7.4.2.2 GaN

Unlike GaAs, GaN is a new photocathode material that promises a more robust NEA material suitable for operating in less stringent vacuum conditions. As a wide band gap material, GaN requires UV illumination. Its large band gap leads to a stronger bonding of Cs to the surface, resulting in a NEA condition with only Cs. Therefore, the main appeal of GaN for accelerator applications is in its more stable Cs layer that may prove beneficial for high current operation, or when the photocathode must be at an elevated temperature. However, it is not expected that the activated layer noticeably would be more forgiving to chemical poisoning gases than GaAs, and therefore, the partial pressures of these species similarly must be small.

The preparation and activation procedures for GaN photocathodes resemble those for GaAs. Likewise, the material is typically strongly p-doped (~1×10^{19} cm^{-3}) to ensure high conductivity and band bending near the surface. However, extensive heat treatment is typically not required, as GaN seemingly is much more inert to oxide formation. For example, a simple vacuum-bakeout to 200 ˚C reportedly restored its QE to 50% of its original value after exposing the photocathode to a nitrogen atmosphere [7.62]. The activation is simpler, as mentioned earlier, with the use of cesium only generating excellent QEs of as high as 50% for simple bulk photocathodes, although requiring a UV spectral range more difficult to attain for the laser and the optics.

7.4.2.3 Tertiary and Other Advanced Structures

Considerable flexibility exists in researcher’s ability to tune the band gap and other parameters for alloys such as $Al_xGa_{1-x}N$, $In_xGa_{1-x}N$, $GaAs_{1-x}P_x$, and $Al_xGa_{1-x}As$. For example, by varying the concentration of In in $In_xGa_{1-x}N$, the band gap can be matched to a laser operating in the visible range while retaining some benefits of GaN material. This can lead to both better QEs and improvements in other parameters relevant to accelerators, such as thermal emittance. Despite the promises of better performances compared to actual NEA photocathodes, those materials have not yet been tested in a real photoinjector. Particular attention must be paid when the semiconductor goes from a direct- to an indirect-band gap material. For example, despite its good QE, $GaAs_{0.55}P_{0.45}$ was found to have a noticeably higher thermal emittance than GaAs at the same laser wavelength, despite its larger band gap [7.63]. An explanation was offered, noting that GaP is an indirect band gap material, and the transition from direct (GaAs) to indirect occurs at about 45% concentration of phosphorus. This implies that additional momentum transfer occurs during photoemission to conserve crystal momentum, so engendering the increased transverse velocities of electrons leaving the surface.

Another common characteristic of more advanced structures is the ability to grow transmission-mode photocathodes on a transparent substrate. For example, the response time of thin films of III-V material can be tailored, even at wavelengths where the temporal tail can be significant for bulk crystal material [7.64]. Further benefits of a transmission-type photocathode may be in its very small thermal emittance, at the sub-thermal level, since the emitted electrons are forced to diffuse toward the surface and undergo scattering within the lattice, thermalizing in the process of doing so (discussed below).

Finally, graded photocathodes are another common approach. Here, the QE can be improved in two ways: First, by increasing the efficiency of light coupling into the material, *e.g.*, through matching the index of refraction of the photocathode and the substrate. For example, a normal bulk GaAs reflects about a third of the incident light, and using the index of refraction matching can better its efficiency by about a factor of three. The second approach is to reflect the electrons inside the material that are traveling away from the surface back to it *via* forming a potential barrier through varying the composition of the tertiary compound. For example, a graded $Al_xGa_{1-x}As$/GaAs photocathode recently demonstrated over 50% quantum efficiency in the green wavelengths [7.65], as depicted in Figure **7.20**.

7.4.3 Photocathode Performance

7.4.3.1 Thermal Emittance

Thermal emittance in NEA photocathodes has been studied in detail. These photocathodes remain the materials of choice when the smallest thermal emittance is required. Figure **7.21** summarizes a typical thermal emittance measurement (or MTE which is related to the thermal emittance) for GaAs obtained from a high voltage DC gun [7.63]. As expected, the thermal emittance is smallest when the photon energy closely matches the energy of the band gap, and increases for higher photon energies.

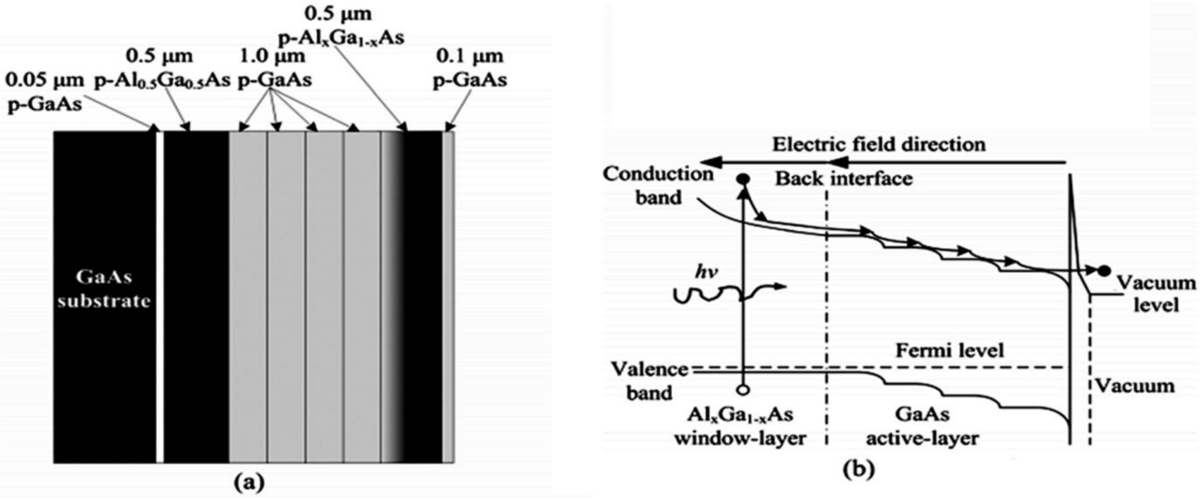

Figure 7.20. An example of advanced transmission-mode graded photocathode that achieves over 30% QE in the transmission-mode and 60% in reflection-mode in the green spectral range. [Reprinted with permission from [7.65]. Copyright 2011, American Institute of Physics.]

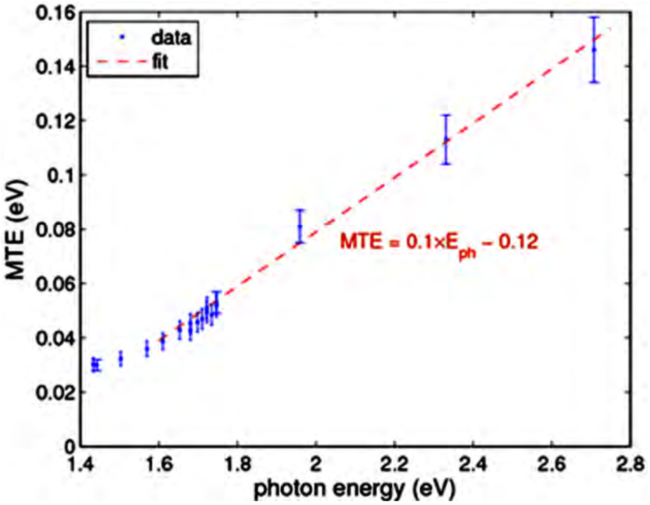

Figure 7.21. Thermal emittance of GaAs photocathode as a function of photon energy. [Adapted with permission from [7.63]. Copyright 2008, American Institute of Physics.]

This result is reproduced routinely in Cornell University's photoinjector operation, and shows remarkable insensitivity to the photocathode's QE. The situation is very different for $GaAs_{0.55}P_{0.45}$ that displayed about 50% variation in MTE when the QE dropped from 6% to 1% (0.200 eV to 0.135 eV, respectively, at 532 nm laser wavelength [7.63]. The explanation behind this, as argued earlier, is because this photocathode has a direct- and indirect-conduction band minimum valley, with emission from the latter being suppressed when the vacuum level is slightly raised (reducing the QE to 1%). We note that the MTE rises with photon energy at a rate slower than $\frac{1}{3}E_{ph}$, as observed in the alkali-based photocathodes, and predicted by Equ. 7.7. This dependence is explained by the fact that a noticeable fraction of electrons escaping into vacuum is fully or partially thermalized down to the conduction band's minimum *via* electron-phonon collisions, or that the emission into the vacuum occurs in a preferential direction close to the surface normal.

So far, only one report of GaN emittance measurements [7.66] at a single laser wavelength (260 nm) has been produced. The result is a surprisingly large MTE = 0.9 eV. In this case, the excess energy is $E_{ph} - E_{gap}$ = 1.4 eV, and assuming a uniform emission into the vacuum hemisphere, the predicted MTE would have been about 1.4/3 = 0.46 eV, *i.e.*, a factor of two smaller. One explanation offered in [7.20] is that the band bending of GaN, which is larger than that in GaAs (1.2 V versus 0.2- to 0.5-V), increased the electrons' kinetic energy before their emission into vacuum. Additional measurements of this type of photocathode are required to arrive at definitive results.

Finally, it is important to point out that the thermal emittance measurements, demonstrated on a weekly basis in the operating photoinjector at Cornell University, as well as the measurements of thermal energy spread at the University of Heidelberg, Germany [7.67], do not reflect the theoretical findings that a very small reduced mass inside these semiconductors (*e.g.*, GaAs Γ-valley electron's effective mass is only $m^* = 0.067m_0$ of its vacuum mass) should lead to a very small transverse velocity after the emission into vacuum, as required by transverse momentum conservation: $m^* v_{\perp,cryst} = m_0 v_{\perp,vac}$. This means that the theory predicts MTE, which can be as small as $kT(m^*/m_0)$, where kT is thermal energy (1/40 eV at 300 K). Indeed, such results were reported by the Stanford group [7.68]. Possible explanations for why several well established groups cannot reproduce this result are the nano-scale roughness of the surface [7.60] or the scattering effect of the activation layer [7.69]. If such low thermal emittances can be reliably realized in photoinjectors, it will open a route toward generating very bright electron beams.

7.4.3.2 Response Time

Response time is another critical parameter for photoinjectors, as the pulse duration needs to be considerably shorter than the wavelength of RF used for acceleration; and also, to allow for laser temporal shaping, which is effective for mitigation of emittance growth of space charge dominated beams. Response of 1 ps or shorter is typically desired. Early results from Max Planck Institute have shown that GaAs excited near the band gap has a long response time with a tail that extends to 100 ps. It was also shown in their work [7.70] that the result can be approximately explained by noting that the response time for diffusing electrons can be written as

$$\tau = \frac{1}{\alpha^2 D} \tag{7.10}$$

where α is the optical absorption constant and D is the electron diffusion coefficient. Because the optical absorption constant varies substantially with the photon wavelength, it is therefore expected that the response time changes by many orders-of-magnitude with a shorter wavelength excitation. Indeed, the measurements performed at Cornell have shown that GaAs is a prompt photoemitter (< 1 ps) when excited with 520 nm laser wavelength. An example of data and comparison with Equ. 7.10 are shown in Figure **7.22**. Generally Equ. 7.10 overestimates the response time. Possible explanations are in the fact that additional recombination processes occurring at the surface are not accounted in this model.

We note that even for excitation with a near band gap photons, GaAs can be made into a fast photocathode in the transmission-mode albeit at the expense of its QE [7.64]. GaN's response time at 260 nm essentially approximated a delta function [7.66]. This is not very surprising given that the material's absorption length is very short at this photon energy.

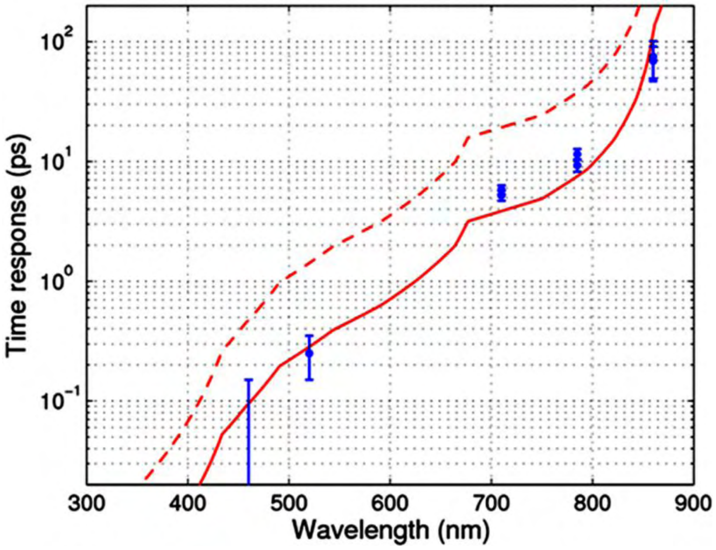

Figure 7.22. Collection of the GaAs photoemission response time measurements [7.18], [7.26] vs. the laser wavelength along with the theoretical predictions (dashed line). Better agreement is obtained for $\tau = (\alpha^{-2} D^{-1})/5$ (solid line). The measurement at 460 nm was only able to place an upper estimate on the response time.

7.4.3.3 High Current Operation

High current operational experience with unpolarized high QE photocathodes mostly is limited to JLAB's experience of IR FEL, DC laser tests performed by the CEBAF injector group, and staff at Cornell University's Energy Recovery Linac photoinjector. The lifetime here depends on many factors, such as DC voltage versus the bunched structure of the beam, charge per bunch, average current, location of the laser spot on the photocathode, scattered laser light, beam losses, and the quality of the beamline's vacuum. For pulsed operation at JLAB FEL, a 1/*e* operational lifetime at 550 Coulombs at 5 mA was demonstrated with GaAs [7.71]. Extensive studies at CEBAF using the DC laser have resulted in 1/*e* lifetime of more than 1000 Coulombs for a 9.5 mA DC beam [7.72], *viz.*, the best for this photocathode operated at high average current. Cornell University's photoinjector can operates with GaAs at 20 mA average current with a 1/*e* lifetime of approximately an hour, with possible causes of this lifetime identified to be from the laser scattering due to rough in-vacuum metallic-polished mirrors, and the generation of beam halos. Figure **7.23** gives an example of beam current. Also, lifetime can be improved by simply moving the laser spot further off-axis since the location of the main damage is confined to the gun's electrostatic center. However, as expected, GaAs demonstrate a much reduced lifetime, as seen in Figure **7.14**, compared to alkali-based photocathodes, such as K_2CsSb. Other possible mechanisms for degrading lifetime are due to the somewhat elevated temperature of the photocathode when the beam is on, and to increased beam losses at higher bunch charges and currents. Additional studies on GaAs at elevated temperatures show a reduced dark lifetime [7.73] that can be resolved through designing efficient cooling of the photocathode in the presence of the incident laser beam.

Finally, we note the importance of the surface charge effect when operating high current, unpolarized NEA photocathodes, a phenomenon first observed when employing at high beam current at the SLAC polarized source using GaAs. Many references are available on this subject [7.74]–[7.76]. Essentially, the effect lies in the resistor-capacitor circuit-like behavior wherein an electron charge excited by the laser pulse is not extracted into vacuum and builds up a potential barrier at the photocathode's surface, causing a time dependent transient of the beam current, even though the laser's intensity stays constant. The effect is most strongly pronounced when the photon energy close to the semiconductor band gap is being used and not heavily p-doped crystals (*e.g.*, as typically required for polarized sources where generally the QE is very low).

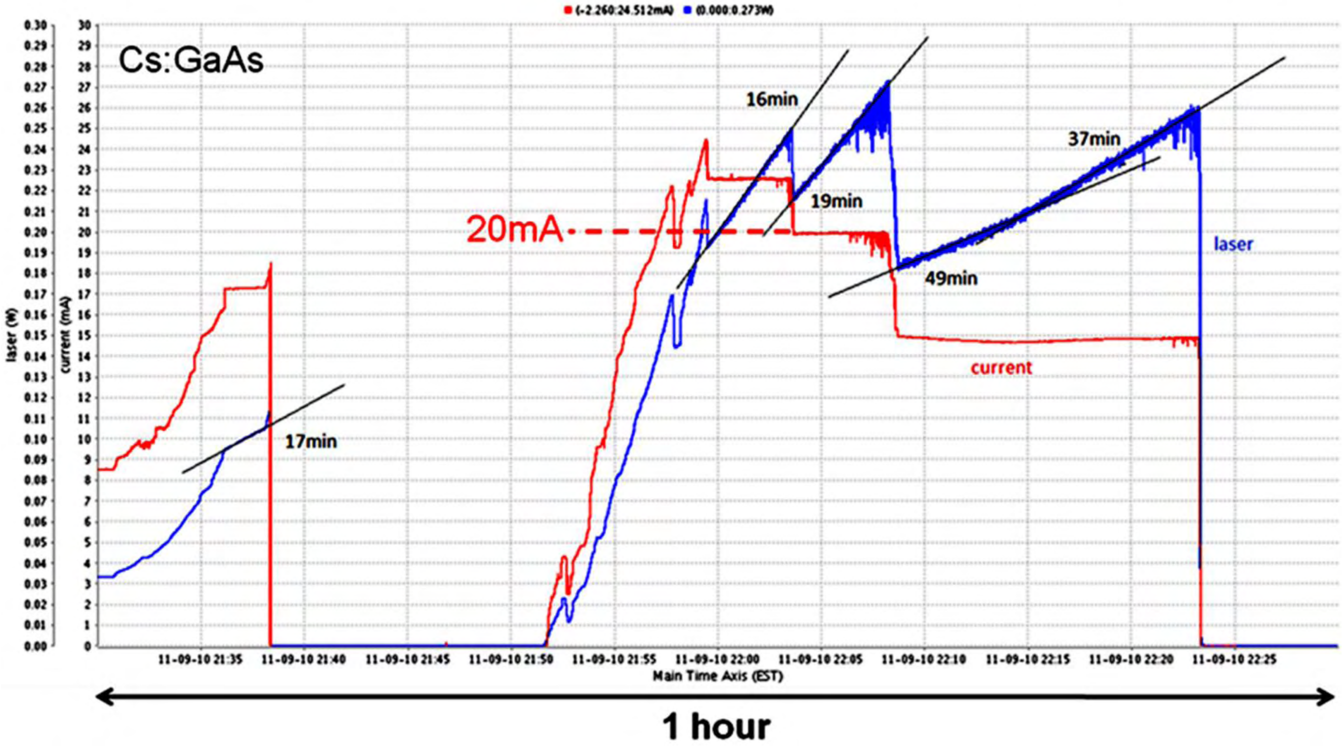

Figure 7.23. An example of GaAs lifetime operated at high current at Cornell University's photoinjector. The laser's slow feedback ensures constant current (red line) by regulating its power (blue line) accordingly. 1/*e* lifetime is indicated for cases where the laser spot was close to the gun's electrostatic center, with the resulting short photocathode lifetime. By moving the spot further off-center, lifetime is increased substantially.

This phenomenon also was observed at Cornell University's ERL photoinjector when operating at high currents, and using highly p-doped GaAs crystal. Employing fast beam current diagnostics with pulsed operation [7.77], revealed a small leading peak, lasting about 0.1 µs, in macropulses with a substantial average current, even though the laser pulse is constant over the macropulse's entire duration (Figure **7.24**). The effect became more pronounced as QE degraded, consistent with the SLAC observations. Overall, the effect played a small role for a 520 nm laser and a reasonable QE for heavily p-doped GaAs, though it can become important during a pulsed operation where the transient due to the leading peak of the surface charge effect may become undesirable.

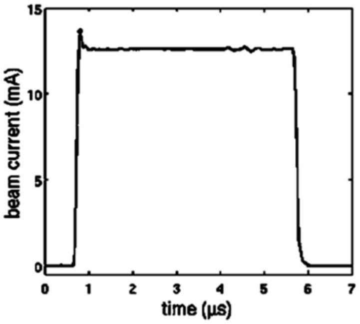

Figure 7.24. An example of surface charge effect in GaAs operated at high average current [7.38]. The laser pulse is constant over the duration of the macropulse.

7.5 CONCLUSION

Semiconductor photocathodes provide viable alternatives for generating average currents exceeding 30 mA with acceptable life time and intrinsic emittance for high average flux FEL and high current collider applications. Average current of > 30 mA, with life time in the order of days, intrinsic emittance of nearly the fundamental limit and response time in the picosecond time range has been generated with K_2CsSb photocathodes. Similar performance with a slightly lower life time, but better intrinsic emittance has been produced with GaAs: Cs cathodes, as well. In the forthcoming years, with better understanding of physical properties controlling their performance, it may be possible to tailor the cathode to suit the application.

7.6 CONFLICT OF INTEREST AND ACKNOWLEDGEMENT

We confirm that this article content has no conflicts of interest and would like to acknowledge the support of the US National Science Foundation and Department of Energy under contract numbers NSF DMR-0807731, DOE DE-SC0003965 and DE-AC02-98CH10886.

References

[7.1] W. E. Spicer, “Photoemissive, photoconductive, and optical absorption studies of alkali-antimony compounds,” *Phys. Rev.*, vol. 112, pp. 114-122, October 1958.

[7.2] I. V. Bazarov, B. M. Dunham and C. K. Sinclair, “Maximum achievable beam brightness from photoinjectors,” *Phys. Rev. Lett.*, vol. 102, pp. 104801-1–104801-4, March 2009.

[7.3] C. K. Sinclair, “High voltage DC photoemission electron guns – current status and technical challenges,” *ICFA Beam Dynamics Newslett.*, vol. 46, pp. 97-118, August 2008.

[7.4] D. H. Dowell I. Bazarov, B. Dunham *et al.*, “Cathode R&D for future light sources,” *Nucl. Instrum. Meth. A*, vol. 622, pp. 685-697, October 2010.

[7.5] Z. Insepov, “Bialkali/multi-alkali response” [Online]. Available FTP: psec.uchicago.edu Directory: library/photocathodes File: zeke_Bialkali.png [Accessed on March 6, 2013].

[7.6] H. Sommer, *Photoemissive Materials: Preparation, Properties, and Uses*, New York: Wiley, 1968.

[7.7] D. H. Dowell, K. J. Davis, K. D. Friddell *et al.*, “First operation of a photocathode radio frequency gun injector at high duty factor,” *Appl. Phys. Lett.*, vol. 63, pp. 2035-2037, October 1993.

[7.8] R. Nathan, C. H. B. Mee, “Photoelectric and related properties of the potassium-antimony-caesium photocathode,” *Int. J. Electron.*, vol. 23, pp. 349-354, October 1967.

[7.9] A. di Bona, F. Sabary, S. Valeri *et al.*, “Auger and x-ray photoemission spectroscopy study on Cs_2Te photocathodes,” *J. Appl. Phys.*, vol. 80, pp. 3024-3030, September 1996.

[7.10] R. A. Powell, W. E. Spicer, G. B. Fisher *et al.*, “Photoemission studies of cesium telluride,” *Phys. Rev. B*, vol. 8, pp. 3987-3995, October 1973.

[7.11] P. Michelato, A. Di Bona, C. Pagani *et al.*, “R&D activity on high QE alkali photocathodes for RF guns,” in *Proc. 1995 Particle Accelerator Conf.*, 1995, pp. 1049-1051.

[7.12] P. Michelato, “Report of high quantum efficiency photocathode at Milano,” in *Proc. AIP Conf.*, vol. 279, 1992, pp. 775-760.

[7.13] L. Cultrera, I. V. Bazarov, A. Bartnik *et al.*, “Thermal emittance and response time of a cesium antimonide photocathode,” *Appl. Phys. Lett.*, vol. 99, pp. 152110-1–152110-3, October 2011.

[7.14] S. M. Johnson, “Optical absorption and photoemission in semitransparent and opaque Cs_3Sb photocathodes,” *Appl. Opt.*, vol. 32, pp. 2262, May 1993.

[7.15] M. Hagino and T. Takahashi, “Thickness of Cs-Sb films relative to the original Sb films,” *J. Appl. Phys.*, vol. 37, pp. 3741-3743, September 1966.

[7.16] P. Michelato, P. Gallina *et al.*, "Alkali photocathode development for superconducting rf guns," *Nucl. Instrum. Methods A*, vol. 340, pp. 176-181, February 1994.

[7.17] Y. Nakazono, M. Kunihiro, A. Sakumi *et al.*, "Upgrade of cartridge-type exchangeable Na_2KSb cathode gun," in *Proc. 2010 Int. Particle Accelerator Conf.*, 2010, pp. 4293-4295.

[7.18] R. W. Engstrom, *Photomultiplier Handbook*, Lancaster, PA: RCA/Burle, 1980.

[7.19] P. Dolizy, "Optical method for investigating alkali antimonide photocathodes," *Vacuum*, vol. 30, pp. 489-495, 1980.

[7.20] B. Erjavec, J. Šetina and L. Irmančnik-Belič, "Modelling of the alkali vapour-pressure dynamics during the epitaxial growth of semi-transparent photo-emissive layers," *Vacuum*, vol. 67, pp. 235-241, September 2002.

[7.21] A. Dubovoi, A. S. Chernikov, A. M. Prokhorov *et al.*, "Multialkali photocathodes grown by molecular beam epitaxy technique," in *Proc. SPIE*, 1991, vol. 1358, pp. 134-138.

[7.22] Natarajan, A. T. Kalghatgi, B. M. Bhat *et al.*, "Role of the cesium antimonide layer in the Na_2KSb/Cs_3Sb photocathode," *J. Appl. Phys.*, vol. 90, pp. 6434-6439, December 2001.

[7.23] W. H. McCarroll, R. J. Paff and A. H. Sommer, "Role of Cs in the $(Cs)Na_2KSb$ (S-20) multialkali photocathode," *J. Appl. Phys.*, vol. 42, pp. 569-572, February 1971.

[7.24] D. H. Dowell, S. Z. Bethel and K. D. Friddell, "Results from the average power laser experiment photocathode injector test," *Nucl. Instrum. Meth. A*, vol. 356, pp. 167-176, March 1995.

[7.25] I. Bazarov, L. Cultrera, A. Bartnik *et al.*, "Thermal emittance measurements of a cesium potassium antimonide photocathode", *Appl. Phys. Lett.*, vol. 98, pp. 224101-1–224101-3, June 2011.

[7.26] T. Vecchione, I. Ben-Zvi, D. H. Dowell *et al.*, "A low emittance and high efficiency visible light photocathode for high brightness accelerator-based X-ray light sources," *Appl. Phys. Lett.*, vol. 99, pp. 034103-1–034103-3, July 2011.

[7.27] A. Braem, E. Chesi, W. Dulinski *et al.*, "Highly segmented large-area hybrid photodiodes with bialkali photocathodes and enclosed VLSI readout electronics," *Nucl. Instrum. Methods A*, vol. 442, pp. 128-135, March 2000.

[7.28] A. Burrill, I. Ben-Zvi, T. Rao *et al.*, "Multi-alkali photocathode development at Brookhaven National Lab for application in superconducting photoinjectors," in Proc. 2005 Particle Accelerator Conf., 2005, pp. 2672-2674.

[7.29] E. Shefer, A. Breskin, A. Buzulutskov *et al.*, "Laboratory production of efficient alkali-antimonide photocathodes," *Nucl. Instrum. Meth. A*, vol. 411, pp. 383-388, July 1998.

[7.30] K. Nakamura, Y. Hamana,Y. Ishigami *et al.*, "Latest bialkali photocathode with ultra high sensitivity," *Nucl. Instrum. Meth. A*, vol. 623, pp. 276-278, November 2010.

[7.31] D. Sertore, P. Michelato, L. Monaco *et al.*, "Review of the production process of TTF and PITZ photocathodes," in *Proc. 2005 Particle Accelerator Conf.*, 2005, pp. 671-673.

[7.32] L. Monaco, P. Michelato, D. Sertore *et al.*, "Multiwavelengths optical diagnostic during Cs_2Te photocathodes deposition," in *Proc. 2010 Int. Particle Accelerator Conf.*, 2010, pp. 1719-1721.

[7.33] A. di Bona, F. Sabary, S. Valeri *et al.*, "Formation of the Cs_2Te photocathode: auger and photoemission spectroscopy study," in *Proc. 1996 European Particle Accelerator Conf.*, 1996, pp. 1475-1477.

[7.34] F. Baumann, J. Kessler and W. Roessler, "Composition of Antimony Evaporating from Different Sources," *J. Appl. Phys.*, vol. 38, pp. 3398-3399, March 1967.

[7.35] H. Sugiyama, H. Kobayakawa, Y. Takeda *et al.*, "Effect of substrate on the quantum efficiency of cesium telluride thin-film photocathodes," *J. Japan Inst. Metals*, vol. 69, pp. 493-496, October 2005.

[7.36] L. Cultrera, I. V. Bazarov, J. V. Conway *et al.*, "Growth and characterization of bialkali photocathodes for Cornell ERL injector," in Proc. *2011 Particle Accelerator Conf.*, 2011, pp. 1942-1944.

[7.37] M. Krasilnikov, "Impact of the cathode roughness on the emittance of an electron beam," in *Proc. 2006 Free Electron Laser Conf.*, 2006, pp. 586-583.

[7.38] D. Sertore, S. Schreiber, K. Flöettmann *et al.*, "First operation of cesium telluride photocathodes in the TTF injector RF gun," *Nucl. Instrum. Meth. A*, vol. 445, pp. 422-426, May 2000.

[7.39] D. Sertore, "Photocathode for FLASH and PITZ: a summary," presented at 1st QE Photocathode RF Guns Workshop, Milan, Italy, October 5, 2006.

[7.40] *Photo-injectors for CTF3 and CLIC: Photocathodes* [Online]. Available: http://photoinjector.web.cern.ch/photoinjector/Photocathodes.htm [Accessed: January 31, 2012].

[7.41] S. Schreiber, P. Michelato, L. Monaco *et al.*, "On photocathodes used at the TTF photoinjector," in *Proc. Particle Accelerator Conf.*, 2003, pp. 2071-2073.

[7.42] D. Sertore, L. Monaco, P. Michelato *et al.*, "High QE photocathodes at FLASH," in *Proc. 2006 European Particle Accelerator Conf.*, 2006, pp. 2496-2498.

[7.43] D. Sertore, P. Michelato, L. Monaco *et al.*, "High quantum efficiency photocathode for RF guns," in *Proc. 2007Asian Particle Accelerator Conf.*, 2007, pp. 223-225.

[7.44] V. Miltchev, J. Bähr, H. J. Grabosch *et al.*, "Measurements of thermal emittance for cesium telluride photocathodes at PITZ," in *Proc. 2005 Free Electron Laser Conf.*, 2005, pp. 560-563.

[7.45] T. Rao, presented at 2011 Energy Recovery Linac, Tsukuba, Japan, October 2011.

[7.46] Femtosecond streak camera C6138 (FESCA-200), available by Hamamatsu Photonics K.K., Hamamatsu, Japan. Available at http://sales.hamamatsu.com/assets/pdf/hpspdf/e_c6138.pdf.

[7.47] T. Nordlund, "Streak Cameras for Time-Domain Fluorescence," in *Topics in Fluorescence Spectroscopy*, 1st Ed., Berlin: Springer-Verlag, 2002, Chap. 3, pp. 183-256.

[7.48] S. H. Kong, J. Kinross-Wright, D. C. Nguyen *et al.*, "Cesium telluride photocathodes," *J. Appl. Phys.*, vol. **77**, pp. 6031-6038, June 1995.

[7.49] K. Miyoshi, K. Kambe, A. Sakumi *et al.*, "Commissioning of Na_3KSb photocathode rf gun in s-band linac at the university of Tokyo," in *Proc. 2009 Particle Accelerator Conf.*, 2009, pp. 587-589.

[7.50] L. Cultrera, J. Maxson, I. Bazarov *et al.*, "Photocathode behavior during high current running in the Cornell energy recovery linac photoinjector," *Phys. Rev. ST Accel. Beams*, vol. 14, pp. 120101-1–120101-12, December 2011.

[7.51] S. Lederer, S. Schreiber, P. Michelato *et al.*, "Photocathode studies at FLASH," in *Proc. 2008 European Particle Accelerator Conf.*, 2008, pp. 232-234.

[7.52] U. Weigel, "Cold intense electron beams from gallium arsenide photocathode," Ph.D. Thesis, Universität Heidelberg, Heidelberg, Germany, 2003.

[7.53] R. L. Bell, *Negative Electron Affinity Devices*, Oxford: Clarendon Press, 1973

[7.54] J. S. Escher, "NEA Semiconductor Photoemitters," in *Semiconductors and Semimetals* vol. 15, Oxford: Clarendon Press, 1981, Chap. 3, pp. 195-300.

[7.55] V. Siklitsky, *New Semiconductor Materials: Characteristics and Properties*, 2001. [Online] Available: http://www.ioffe.ru/SVA/NSM/ [Accessed: January 9, 2011].

[7.56] Z. Liu, "Surface characterization of semiconductor photocathode structures," Ph.D. Thesis, Stanford University, Stanford, California, 2005.

[7.57] X. Liu, unpublished.

[7.58] A. Guillén-Cervantes, Z. Rivera-Alvarez, M. López-Luna *et al.*, "GaAs surface oxide desorption by annealing in ultra high vacuum," *Thin Solid Films*, vol. 373, pp. 159-169, September 2000.

[7.59] S. Karkare, I. Bazarov, L. Cultrera *et al.*, "Effect of surface roughness on the emittance from GaAs photocathode," in *Proc. 2011 Particle Accelerator Conf.*, 2011, pp. 2480-2482.

[7.60] S. Karkare and I.V. Bazarov, "Effect of nano-scale surface roughness on transverse energy spread from GaAs photocathodes," *Appl. Phys. Lett.*, vol. 98, pp. 094104-1–094104-3, March 2011.

[7.61] Z. Liu, Y. Sun, S. Peterson *et al.*, "Photoemission study of Cs-NF_3 activated GaAs(100) negative electron affinity photocathodes," *Appl. Phys. Lett.*, vol. 92, pp. 241107-4–241107-3, June 2008.

[7.62] O. Siegmund, J. Vallerga, J. McPhate *et al.*, "Development of GaN photocathodes for UV detectors," *Nucl. Instrum. Meth. A*, vol. 567, pp. 89-92, November 2006.

[7.63] I. V. Bazarov, B. M. Dunham, Y. Li *et al.*, "Thermal emittance and response time measurements of negative electron affinity photocathodes," *J. Appl. Phys.*, vol. 103, pp. 054901-1–054901-8, March 2008.

[7.64] K. Aulenbacher, J. Schuler, D. v. Harrach *et al.*, "Pulse response of thin III/V Semiconductor photocathodes," *J. Appl. Phys.*, vol. 92, pp. 7536-7543, December 2002.

[7.65] Y. Zhang, B. Chang, J. Niu *et al.*, "High-efficiency graded band-gap $Al_xGa_{x-1}As$/GaAs photocathodes grown by metalorganic chemical vapor deposition," *Appl. Phys. Lett.*, vol. 99, pp. 101104-1–101104-3, September 2011.

[7.66] I. V. Bazarov, B. M. Dunham, X. Liu *et al.*, "Thermal emittance and response time measurements of a GaN photocathode," *J. Appl. Phys.*, vol. 105, pp. 083715-1–083715-4, April 2009.

[7.67] D. A. Orlov, M. Hoppe, U. Weigel *et al.*, "Energy distributions of electrons emitted from GaAs (Cs, O)," *Appl. Phys. Lett.*, vol. 78, pp. 2721-2723, April 2001.

[7.68] Z. Liu, Y. Sun, P. Pianetta and R. F. W. Pease, "Narrow cone emission from negative electron affinity photocathodes," *J. Vacuum Sci. Technology B*, vol. 23, pp. 2758-2762, December 2005.

[7.69] D. C. Rodway and M. B. Allenson, "*In* situ surface study of the activating layer on GaAs (Cs, O) photocathodes," *J. Physics D: Appl. Physics*, vol. 19, pp. 1353-1371, July 1986.

[7.70] P. Hartman, J. Bermuth, D. v. Harrach *et al.*, "A diffusion model for picosecond electron bunches from negative electron affinity GaAs photocathodes," *J. Appl. Phys.*, vol. 86, pp. 2245-2249, August 1999.

[7.71] C. Hernandez-Garcia *et al.*, "Status of the Jefferson Lab ERL FEL DC photoemission gun," in *Proc. 2009 Energy Recovery Linac*, 2009, pp. 37-39.

[7.72] J. Grames, R. Suleiman, P. A. Adderley *et al.*, "Charge and fluence lifetime measurements of a dc high voltage GaAs photogun at high average current," *Phys. Rev. ST Accel. Beams*, vol. 14, pp. 043501-1–043501-12, April 2011.

[7.73] H. Iijima, C. Shonaka, M. Kuriki *et al.*, "A study of lifetime of NEA-GaAs photocathode at various temperatures," in *Proc. 2010 Int. Particle Accelerator Conf.*, 2010, pp. 2323-2325.

[7.74] M. Woods, J. Clendenin, J. Frisch *et al.*, "Observation of a charge limit for semiconductor photocathodes," *J. Appl. Phys.*, vol. 73, pp. 8531-8535, June 1993.

[7.75] G. A. Mulhollan, A. V. Subashiev *et al.*, "Photovoltage effects in photoemission from thin GaAs layers," *Phys. Lett. A*, vol. 282, pp. 309-318, April 2001.

[7.76] H. Tang, R. K. Alley, H. Aoyagi *et al.*, "Study of nonlinear photoemission effects in III-V semiconductors," in *Proc. 1993 Particle Accelerator Conf.*, 1993, pp. 3036-3038.

[7.77] F. Loehl, private communication.